

Major Qualifying Project Report  
Palladium On Carbon Catalyst



Submitted to:

Sunovion Pharmaceuticals Inc.

&

Chemical Engineering Faculty of  
WORCESTER POLYTECHNIC INSTITUTE

Authors:

Jonathan McIntyre

Yuhan Yang

Kofi Colecraft

Approved By:

---

---

# Abstract

It is of utmost importance for pharmaceutical companies to fully understand their drug production process. Sunovion Pharmaceuticals identified their heterogeneous palladium on carbon catalyst as a strategic area to enhance efficiency by establishing superior catalyst characterization. A device was designed, constructed, and validated for determining the surface area and dispersion of the catalyst by chemisorption, in addition to Scanned Electron Microscopy and Brunauer Emmett Teller techniques. Moreover, mass diffusion limitations were identified based on presence of microporous graphite carbon support and tested by zero length column analysis and temperature programmed desorption. Formal recommendations are proposed to direct the future use of precious metal catalysis by Sunovion.

# Acknowledgments

**We would like to thank Professors Andrew Teixeira and Stephen Kmiotek for their guidance throughout this project. We would like to thank Mr. Robert Prytko, and Sunovion Pharmaceuticals for giving us this opportunity to work on a great chemical engineering project. We would also like to thank the WPI chemical engineering M.S. student Jim Vicens, for the extra support and encouragement in the lab.**

# Table of Contents

<b>Abstract</b>	<b>1</b>
<b>Acknowledgments</b>	<b>2</b>
<b>Table of Figures</b>	<b>5</b>
<b>Table of Tables</b>	<b>7</b>
<b>Authorship Page</b>	<b>7</b>
<b>Introduction</b>	<b>10</b>
<b>Background</b>	<b>12</b>
2.1 General Scope of Catalysis	12
2.2 Homogeneous vs. Heterogeneous Catalysts	13
2.3 Palladium as a Catalyst	15
2.4 Catalyst deactivation	16
2.5 Support Structures	18
2.5.1 Carbon as a Support	20
2.6 Palladium on Carbon	22
2.6.1 Pd/C applications	23
2.7 Typical Analytical Methods	25
2.7.1 Chemisorption	25
2.7.2 Physisorption	25
2.7.3 Temperature-programmed Reduction	26
2.7.4 SEM Analysis	27
2.7.5 TEM Analysis	28
2.7.8 XRD Analysis	29
2.7.9 X-Ray Photoelectron Spectroscopy (XPS)	30
2.7.10 Diffuse Reflection Infrared Spectroscopy (DRIFTS)	31
2.7.11 Inductively Coupled Plasma Spectroscopy (ISP)	32
2.7.12 Zero Length Column Technique (ZLC)	33
<b>Methods</b>	<b>34</b>
3.1 Calibration	34
3.2 Pulse Titration	36
3.2.1 Equipment Setup	36
3.1.2 Theory	38
3.1.3 Procedure	40
3.2 Zero Length Column	44
3.2.1 Procedure	44

3.3 TPD	44
3.4 SEM	45
3.5 BET	47
3.6 Safety	48
<b>Results</b>	<b>50</b>
4.1 SEM	50
4.2 Pulse Titration	50
4.2.1 Molar Amount of Hydrogen Adsorbed	50
4.2.2 Surface Area and Dispersion	52
4.3 ZLC	53
4.4 TPD	54
<b>5. Discussion</b>	<b>55</b>
5.1 Mass Diffusion Limitation	55
5.2 Surface Area Characterization	57
5.3 Dispersion Characterization	58
<b>6. Error Analysis</b>	<b>60</b>
6.1 Pulse Titration	60
<b>7. Conclusions</b>	<b>63</b>
<b>8. Appendix</b>	<b>65</b>
8.1 Titration Calculations	65
8.2 Titration Data Excerpt	66
8.3 SEM	68
8.4 Valve Configurations	71
8.5 MatLAB Script	72
Finding Beta%%	74
solving for diffusivity %%	76
8.6 Chemisorption Graphs	77
<b>9. References</b>	<b>79</b>

# Table of Figures

## Background

Figure 1 Free Energy v. Reaction Coordinate. (Pearson, 2002)	13
Figure 2 Comparison of SEM image of Pd catalyst. (Journal of Materials Chemistry)	14
Figure 3 Temperature Range of Catalytic Metals. (Chorkendorff, 2015)	18
Figure 4 Comparison of uses of Pd/C catalyst (Chemistry LibreTexts).	23
Figure 5 Schematic of catalytic hydrogenation. (Chemistry LibreTexts).	24
Figure 6 Comparison of different types of BET graphs. (Thorsten Wagner, 2011)	26
Figure 7 Comparison of TPR profiles. (Amorim & Keane, 2008)	27
Figure 8 Comparison of SEM images (Sarioglan, 2013).	28
Figure 9 Comparison of TEM images (Heidenreich 2001).	28
Figure 10 Comparison of XRD analysis (Sarioglan, 2013).	29
Figure 11 XPS scan of a Rhodium catalyst. (Chorkendorff. Pg. 136)	31
Figure 12 Comparison of radiation and transmission spectrum (T. Armaroli, 2004).	32
Figure 13 Schematic of the ZLC and Chamber	33

## Methodology

Figure 14 Calibration data	34
Figure 15 Calibration data with higher injection volume	35
Figure 16 Calibration curve of Pulse Titration	36
Figure 17 GC System Schematic.	37
Figure 18 A temperature variance outline of 40C	41
Figure 19 Four minutes injection profile of 40C	42
Figure 20 TPD profiles	45
Figure 21 Comparison of SEM images of Pd/c	46
Figure 22 Comparison of SEM images of Pd/c	46

<b>Figure 23</b> BET profile of test catalyst.	<b>48</b>
<b>Figure 24</b> Schematic of Bubbler System for system safety.	<b>49</b>

## **Results**

<b>Figure 25</b> Comparison of SEM images of Pd/c	<b>50</b>
<b>Figure 26</b> Normalized and averaged Chemisorption data (Fresh catalyst)	<b>51</b>
<b>Figure 27</b> Normalized and averaged Chemisorption data (Spent catalyst)	<b>52</b>
<b>Figure 28</b> Chemisorption Injection time Variation	<b>52</b>
<b>Figure 29</b> Raw data of ZLC method	<b>54</b>
<b>Figure 30</b> TPD Profiles	<b>54</b>

## **Error Analysis**

<b>Figure 31</b> Standard way of manual integration	<b>60</b>
-----------------------------------------------------	-----------

## **Appendix**

<b>Figure 32</b> SEM images under various scales	<b>68</b>
<b>Figure 33</b> SEM images under various scales	<b>69</b>
<b>Figure 34</b> SEM images under various scales	<b>69</b>
<b>Figure 35</b> SEM images under various scales	<b>69</b>
<b>Figure 36</b> Comparison of Chemisorption Valve Configurations	<b>71</b>
<b>Figure 37</b> Comparison of Chemisorption 10 Port Valve Configurations	<b>71</b>
<b>Figure 38</b> Comparison of ZLC Valve Configurations	<b>71</b>

# Table of Tables

## Background

Table 1 Excerpts Hetero and Homogeneous Catalysis uses (Catalysis in Industry, 2013)	15
Table 2 Carbon support advantages (American Chemical Society)	21
Table 3 Comparison of Palladium Catalyst characteristics (American Chemical Society)	22

## Results

Table 4 Comparison of Sunovion Literature and experimental results.	53
Table 5 Average diffusivity of each run	53
Table 6 Average amount of Hydrogen injected for each Titrations	66
Table 7 Valve Injection Time - Further Mass Limitation Testing	67
Table 8 SEM image Percent Error	70

# Authorship Page

Section Title	Primary Author(s)	Primary Editor(s)
Abstract	Jon	All
Acknowledgments	All	All
Table of Figures	Yuhan	Yuhan
Table of Tables	Yuhan	Yuhan
Introduction	Kofi	All

<b>Background</b>	All	All
2.1 General Scope of Catalysis	Jon	All
2.2 Homogeneous v. Heterogeneous Catalysts	Yuhan	All
2.3 Palladium as a Catalyst	Kofi	All
2.4 Catalyst deactivation	Yuhan, Kofi	All
2.5 Support Structures	All	All
2.5.1 Carbon as a Support	Kofi	All
2.6 Palladium on Carbon	Kofi	All
2.6.1 Pd/C applications	Yuhan	All
2.7 Typical Analytical Methods	Jon	All
2.7.1 Chemisorption	Jon	All
2.7.2 Physisorption	Jon	All
2.7.3 Temperature-programmed Desorption	Jon	All
2.7.4 SEM Analysis	Jon	All
2.7.5 TEM Analysis	Jon	All
2.7.8 XRD Analysis	Jon	All
2.7.9 X-Ray Photoelectron Spectroscopy (XPS)	Jon	All
2.7.10 Diffuse Reflection Infrared Spectroscopy (DRIFTS)	Jon	All
2.7.11 ICP	Jon	All
2.8.12 ZLC	Jon	All
<b>Methods</b>	All	All
3.1 Calibration	Yuhan	All
3.1 Pulse Titration	Jon	All
3.1.1 Equipment Setup	Jon	All
3.1.2 Theory	Jon	All
3.1.3 Procedure	Jon	All

3.3 Zero Length Column	Jon	All
3.4 TPD	Yuhan	All
3.5 BET	Yuhan	All
3.6 Safety	Kofi	All
<b>Results</b>	All	All
4.1 SEM	Kofi	Yuhan
4.2 Pulse Titration	Jon	Jon
4.2.1 Molar Amount of Hydrogen Adsorbed	Jon	Jon
4.2.2 Surface Area and Dispersion	Jon	Jon
4.3 ZLC	Yuhan	All
4.4 TPD	Yuhan	All
<b>Discussion</b>	Yuhan, Jon	Jon
5.1 Mass Diffusion Limitation	Jon	Jon
5.2 Surface Area Characterization	Jon	Jon
5.3 Dispersion Characterization	Jon	Jon
<b>Error Analysis</b>	Yuhan, Jon	Yuhan, Jon
6.1 Pulse Titration	Yuhan	Jon
<b>Conclusions</b>	Jon	All
<b>Appendix</b>	All	All
8.1 Titration Calculations	Jon	Yuhan, Jon
8.2 Titration Data Excerpt	Jon, Yuhan	Yuhan
8.3 SEM	Kofi	Yuhan
8.4 Valve Configurations	Yuhan	Yuhan
8.5 MatLAB Script	Jon	Jon

# 1. Introduction

Catalysis plays a significant role in the world's economy by playing a vital role in the majority of chemical processes. Catalysis is present in a variety of industries, which include chemical, petroleum, agriculture, polymer, and electronics. There is an abundance of benefits that are derived from the use of catalysis including reduced waste production, reduced cost, time saving, and increased efficiency.

The rise in the need for catalysis in the pharmaceutical industry was a result of a few inter-related causes. The first cause was the increasing regulatory requirements and demand in pharmaceutical products. Over the past few decades major stakeholders in the pharmaceutical industries are creating more stringent rules on the regulation and production of drugs (Thomas,2012)..

Another major reason was the increase in environmental protection in chemical production, or what is commonly referred to as green chemistry. Green chemistry is becoming important to many of the industries that is essential to human development. Green chemistry aims at reducing the use of aggressive, corrosive, or hazardous reagents that have been used more traditionally in industrial production (Thomas,2012).

The move towards using more green chemistry in manufacturing makes catalysis a fundamental and important driver for the shift. The increased need for production of drugs as drugs have become more demanding also caused an increased pressure to reduce drug development cost and time(Thomas,2012).. The last cause of the rise for the need of catalysis in the pharmaceutical industry is the discovery of new practical and functional catalysts from industry and the scholastic sectors. All of these causes

have resulted in the modern prevalence of catalysis in pharmaceutical research, development, and production (Busacca, 2011).

With the growing impact of manufacturing in the pharmaceutical industry catalysis has become increasingly important to the industry. Catalysis is an important technology that provides both economic and environmental benefits to the manufacturing process (Busacca, 2011). With the production of catalytic technologies for use in the pharmaceutical industry can provide the industry access to quicker, cleaner, and more efficient drug delivery to its consumers. It is important to research catalysis and how it can be applied to the different pharmaceutical industries across the globe. Sunovion Pharmaceuticals mission statement is to lead the way to a healthier world by putting patients at the center. Their catalyst was underperforming and was not performing efficiently. Our goal in this project was provide data to help Sunovion by characterizing the surface area and dispersion of their palladium catalyst thus aiding them to achieve their focus on their customer value. This paper focuses specifically on Palladium on Carbon as a catalyst and its implications and applications for use in the pharmaceutical industry and for Sunovion pharmaceuticals.

## 2. Background

### 2.1 General Scope of Catalysis

Catalysts are materials that allow chemical reactions to proceed towards a mechanism that is more energetically favorable, meaning faster reaction speeds and more favorable operating conditions. Catalysts may also allow for selectivity by decreasing side reactions that produce unwanted byproducts and pollutants. About 90% of the chemical industry utilizes catalysis to produce their products. Catalysts are unavoidable in the production of transportation fuels, bulk and fine chemicals, and in the reduction of pollution namely in exhaust systems e.g. catalytic converters in automobile exhaust pipes. Catalyst range from simple molecules to enzymes and from round particles to solid surfaces (Chorkendorff, 2015).

The typical process of a catalytic reaction is a summation of these elementary steps. First, the reactants interact with the catalyst by bonding spontaneously, at which point free energy is released exothermically. The two reactants with slightly altered stereochemistry at a lower energy state now react with each other. This step also requires activation energy, but much less than a non-catalyzed reaction. Lastly, the formed products separate from the catalyst in an endothermic step, but leaves the catalyst completely unchanged with the ability to repeat the process at that site location on the catalyst (Chorkendorff, 2015). *Figure 1* below shows the downsizing of energy required for a reaction to take place.

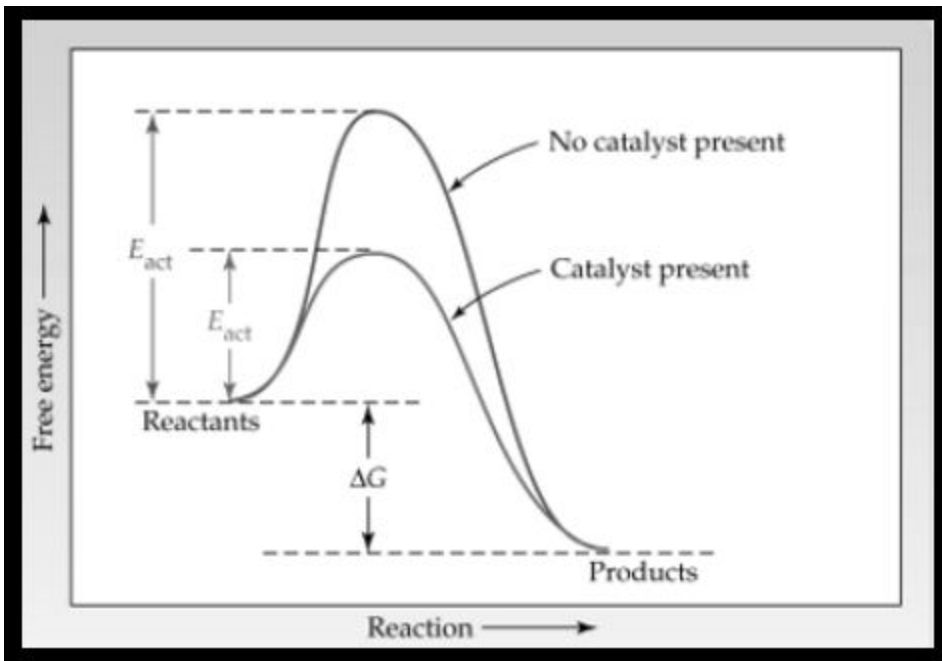


**Figure 1: Free Energy v. Reaction Coordinate** shows free energy changes when catalyst is presented (Pearson, 2002)

The importance of lowering the activation energy is paramount to being able to produce desired products under conditions that are typically safer, for example operating under temperatures closer to regular room temperatures since the reaction requires less heat input. Since less energy input is required, the decreasing activation energy,  $E_{act}$  means faster kinetics and less time is also required to produce the product. So, the monetary value is increased due to the downsizing of production time. Catalyst also make the process cheaper since the equipment can be built and rigged to less extreme conditions that it now can operate at.

## 2.2 Homogeneous vs. Heterogeneous Catalysts

Catalysts can be categorized into two general groups: homogeneous and heterogeneous. Homogeneous catalysts are always in the same phase with reactants, which are typically gases or liquids. Heterogeneous catalysts are in a different phase

than the reactants, normally solid with the reactants are in gas or liquid phase. Homogeneous catalysts normally exist as compounds, particles or simple substances, while heterogeneous catalysts are an activated substance, typically a noble metal, which is supported by another substance. This support structure is typically inert and can be manipulated to provide different capabilities which will be discussed later on. Noble metals are often expensive with cost ranging from \$32 per gram of platinum to \$43 per gram for gold (BASF, 2017). Furthermore, they are hard to separate out of the product cheaply if they are in the same phase as the product. This is the main reason that heterogeneous catalysts exist. (Chorkendorff,2015). *Figure 2.* below shows a heterogeneous and homogeneous catalyst comparison.

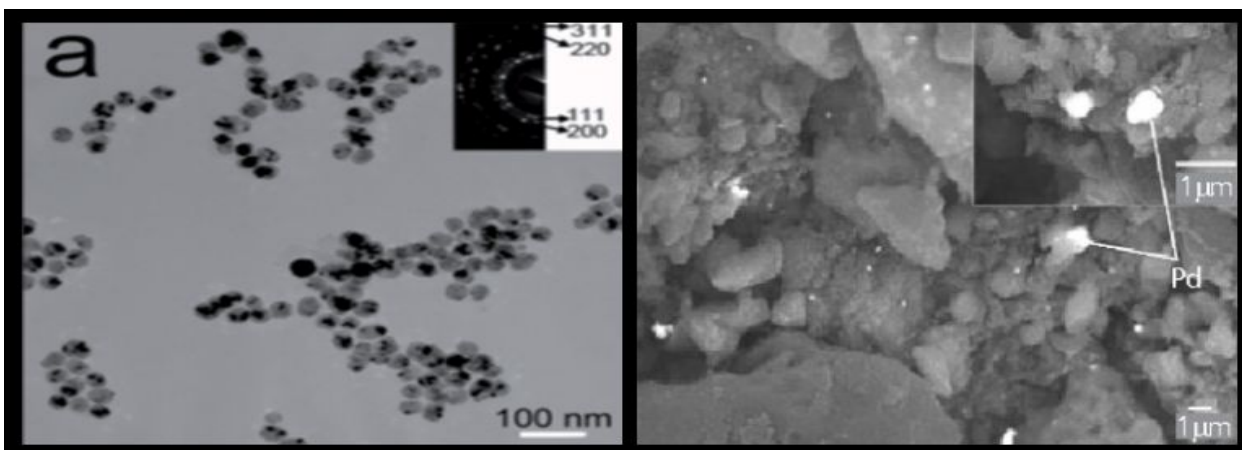


**Figure 2: Comparison of SEM image of homogeneous and heterogeneous Pd catalyst. Left.** homogeneous Pd (Journal of Materials Chemistry); **Right.** heterogeneous Pd on Activated Carbon (Sariođlan).

*Table 1* below provides an elementary description of the types of reactions that utilize different phases of catalyst.

Table 1: Excerpts Hetero and Homogeneous Catalysis uses in industry (Catalysis in Industry, 2013)

<b>Process</b>	<b>Catalyst Type</b>
Production of Ammonia, Sulfuric and Nitric Acid	Heterogeneous
Catalytic Cracking/Alkane Cracking	Heterogeneous
Decomposition for Phenol and Propanone Production	Homogeneous
Alcohol production. e.g. Ethane-1,2-diol.	Homogeneous

## 2.3 Palladium as a Catalyst

Palladium is a versatile metal that is often utilized in organic synthesis. In heterogenous and homogenous catalysis palladium plays an essential role in its effects on organic transformations. Due to this role palladium maintains is essential in the production of bulk and fine chemicals (Gmelin, Preface 1986). It is often used in processes and applications in the production of polymers, agrochemicals, natural products, and pharmaceuticals. Due to its high functional group tolerance, palladium has the capability to participate in a wide variety of catalytic transformations. Palladium catalysts are able to provide good stereo and regio specificity which eliminates the need of protecting groups(Sigma Aldrich, 2017). Protecting groups are typically used in synthesis to shield delicate organic compounds by temporarily masking the parts of the compounds that interfere with the synthesized reaction (Ian Hunt, 2017). Certain parts in organic molecules cannot survive required reagents of chemical environments and protecting groups are used to protect these parts. With palladium there is no need for these protecting groups as palladiums versatility makes it applicable to diverse

types of reaction conditions where there are changes in temperature, solvents, ligands, bases, and other additives (Sigma Aldrich, 2017).

## 2.4 Catalyst deactivation

Catalyst deactivation is the process by which a catalyst loses its selectivity or catalytic activity over a period of time. The deactivation of catalysts is related to several characteristics of the support and the catalyst itself. There are various mechanisms of catalyst deactivation that can be considered. One method of catalyst deactivation is the movement of atoms such that the active sites become covered and are effectively neutralized. This depends on the reacting environment. This method is the process called sintering or agglomeration which is an important reason for catalyst deactivation.

In catalysts that contain a metal support the deactivation is shown through either loss of active metal area, or decrease of catalyst support area (Boskovic, 2004). Different conditions may make the catalyst more or less susceptible to deactivation. Stability also varies with the surface geometry since the structure of support surface dictates how the particles connect. According to Moulijin et al. the nanometer-sized particles are like larger scale particles, a “valley” position that locks the catalyst particle on the surface would highly improve the deactivation and increase the durability of the catalyst. Temperature is the last main contributor to catalyst deactivation. Three main temperature points introduce the most movement to deactivation. The three points are: melting point  $T_{\text{Melting}}$ , and  $T_{\text{Huttig}}$  which is 0.3 of melting point, last one would be  $T_{\text{Tamman}}$  which is 0.5 of melting temperature. (J.A Moulijin) At  $T_{\text{Huttig}}$  the particles would start to cause a drastic increase on mobility compared to normal temperature, then when particles reach  $T_{\text{Tamman}}$  decomposition begins. From the figure below, see *Figure 3*, Pd is relatively stable temperature-wise, which has advantage during sintering.

Good characteristics of a catalyst go far beyond having a good selectivity for the desired product and a high number of active sites. An applicable catalyst must also have a sufficiently long life time relative to its deactivation, be able to be prepared and synthesized reasonably, and have a required thermal and mechanical strength to ward off structural change and collapsing in the catalyst bed respectively. In industry it is also important for the catalyst to be shaped into the proper geometric form to avoid increased pressure gradients of the catalyst bed (Chorkendorff, 2015).

Coking is a form of catalyst deactivation that primarily occurs with catalytic reactions involving hydrocarbons or carbon oxides. In this mechanism side reactions occur on the surface of the catalyst which often lead to the creation of coke, or carbonaceous residues, that tend to cover the active surface of the catalyst (Forzatti, 1999). Fouling is another term often used to describe this process, but that term is often used to describe any type of deposition that might occur on the catalyst surface. Fouling is also typically the physical deposition of species from the fluid phase that might fall onto catalytic surfaces or catalyst pores (Argyle, 2015).

Another type of catalyst deactivation is poisoning. In this mechanism there is a strong chemisorption on the active sites of the catalyst as a result of various impurities that may be present in the feed stream (Forzatti, 1999). A poison is a any molecule derived from a reactant, product, or impurity, with a certain attraction to the catalyst. The mechanism of poisoning can occur by obstructing a catalyst active site or by also altering the adsorption activity of other species(Forzatti, 1999).

Compound	$T_{\text{melting}}$	$T_{\text{Tamman}}$	$T_{\text{Hüttig}}$
Pt	2028	1014	608
PtO	823	412	247
PtO <sub>2</sub>	723	362	217
PtCl <sub>2</sub>	854 <sup>c</sup>	427	256
PtCl <sub>4</sub>	643 <sup>c</sup>	322	193
Pd	1828	914	548
PdO	1023 <sup>c</sup>	512	307
Rh	2258	1129	677
Rh <sub>2</sub> O <sub>3</sub>	1373 <sup>c</sup>	687	412
Ru	2723	1362	817
Fe	1808	904	542
Co	1753	877	526
Ni	1725	863	518
NiO	2228	1114	669
NiCl <sub>2</sub>	1281	641	384
Ni(CO) <sub>4</sub>	254	127	76
NiS	1249	625	375
Ag	1233	617	370
Au	1336	668	401
Cu	1356	678	407

**Figure 3:** Temperature Range of Catalytic Metals (Chorkendorff, 2015)

## 2.5 Support Structures

Catalyst supports serve as a mode of delivery of catalytic substances to aid chemical process. Typically an active catalytic material is implanted onto a an inert support. In Pd/C's case, the palladium is impregnated within the carbon. The effect that the support structure has is it increases the number of catalytic regions available with the component. Catalyst supports are so important because they facilitate the reaction mechanism by providing a controlled surface area with a particular surface chemistry ( Globalspec, 2017). The chemical properties of the structures is dependent on the

dimension, shape, and overall composition of the catalyst support. Suitable media include alumina and silica as well as different types of carbon. Different types of support would increase the particle surface area for various extent, modifies the catalyst selectivity, and minimize the loss of catalyst. The most common and reliable support for catalyst is carbon which would mainly increase the surface area, absorb oxygen and impurities. Alumina is another type of catalyst support that could absorb impurities but would not be able to increase the surface area. Varying pH of Alumina could modulate the selectivity of alumina supported catalyst. Alkaline earth carbonates are other common catalyst supports that could impart basicity and in some cases impedes polymerization of alkynes.

Since catalysis heavily depends on the surface area and the number of active sites, the smaller the active particles typically the more ideal the catalyst is. Smaller particle size, however, results in structure instability and can be susceptible to sintering. In order to combat this, the catalyst is typically placed inside a porous inert support material. Good characteristics of supports are straightforward: Thermal and surface area stability, and strong mechanical strength to resist crushing and fatigue as discussed previously. Pores can vary in size and are ranked from micro (<2 nm) to meso (2-50 nm) to macro (>50 nm) (Chorkendorff, 2015).

There are two methods of preparing a supported impregnation and coprecipitation. The first method is to treat the support (normally solid state) a kind of precatalyst and then activate it under a specific condition to make the precatalyst become a active state. The second method is prepared from homogeneous catalyst. The first method leads to an ideal structure of the catalyst support to be sphere, not necessarily to be perfectly round. Under this state, the catalyst would be more active than the normal precatalyst state. (Peter Munik, 2015)

### 2.5.1 Carbon as a Support

The reason why activated carbons are used as supports for noble metals are due to their large surface area and low intrinsic chemical activity (Suh, Park, Ihm, 1992). They are typically amorphous solids with large pore volumes. Activated Carbon supports typically have pore volumes ranging from  $0.6\text{cm}^3$  per gram to  $2\text{cm}^3$  per gram (Lam,2014) . Such volumes allow for large adsorption capacity. Activated Carbons are relatively inexpensive and provide a high surface area for which the catalyst can be dispersed onto. Along with its high surface area and relatively low costs it is a widely available material. This high surface area that carbon provides as a catalytic support makes it an ideal option for use in catalysis uses and as support to Palladium.

Carbon is used as a support for noble metals such as palladium because it makes the recovery process of the expensive metals relatively easy compared to other widely used supports such as silica and alumina ( $\text{Al}_2\text{O}_3$ ). Silica, despite being easy to manipulate structure size, has the tendency to form contaminants since it has a lower thermal stability. Alumina, offers both thermal and mechanical stability but cannot typically compete with carbon for recoverability of noble metals (Chorkendorff, 2015).

Carbon is used as a catalyst support because of its large specific area, high porosity, high electron conductivity, and relative chemical inertness. Other Important properties that make carbon a great support material in comparison to other materials is its, pore distribution, large volumetric adsorption capacity, electron conductivity, relative chemical inertness. (Lam,2014). In reactions carbon has the potential to be used alongside metallic nanoparticles and enzymes in order to improve catalytic activities. Due to its highly porous nature carbon materials in catalytic reactions exhibit high reactivity due to the additional surface area found within the numerous pores (Lam, 2014). *Table 2* below displays the advantages of carbon as a catalytic support.

**Table 2:** Carbon Support Advantages (Taken from American Chemical Society)

<b>Key Advantages of Carbon Support in Catalytic Applications</b>
1. Resistance to Acidic or Basic Media
2. Tailored pore size distribution for specific reactions
3. Amphoteric character due to the presence of various oxygenated functional groups which enhance metal adsorption and catalyst dispersion
4. Stable structure at high temperatures (even above 1000k), In the presence of oxygen >500 K, and in hydrogenation reactions >700K
5. Less expansive compared to alumina and silica supports
6. Porous carbons can be prepared in different physical forms (granules, extrudates, pellets, fibers, cloths)
7. Hydrophobic carbon can be modified to increase the hydrophilicity
8. Active Phase can be recovered by eliminating the support through burning away the carbon

The carbon support structure can be strategically varied resulting in dramatic effects of the catalyst's operative qualities. Different porosity and positions of the carbon structure will allow or bar certain sized molecules allowing for a select amount of surface area to be targeted. An example of this is apparent in the work of (XYZ) as their Brunauer Emmett Teller (BET) analysis yielded contrary data to the hydrogen uptake. Brunauer Emmett Teller (BET) is a common analysis technique performed by utilizing physisorption to measure the entire surface area of the catalyst, typically done with nitrogen at low temperatures, which will be described in more detail later on. Nitrogen has a covalent bond diameter of 140 picometers which is roughly one half of the distance between stacked graphite sheets. Graphite microporous material by nature, is susceptible to nitrogen being unable to escape its pores resulting in a buildup of pressure, leading to condensation of nitrogen within. Due to this, BET is perhaps an unreliable method for determining surface area for this layered support type. Looking at *Table 3*, an excerpt from Amorim and Keane 2008, it is clear that hydrogen uptake is high for graphite even with a substantially smaller surface area according to BET.

Hydrogen being a much smaller molecule is more likely able to fit in between the graphite sheets.

**Table 3:** Comparison of Palladium Catalyst characteristics with different carbon support structures (Taken from American Chemical Society)

Sample	Hydrogen uptake (cm <sup>3</sup> gPd <sup>-1</sup> )	Pd particle size range (nm)	Standard Deviation of the mean	BET surface area (m <sup>2</sup> /g)
Pd/Activated Carbon	1	1-125	0.2	875
Pd/Graphite	2.2	1.-70	0.1	11
Pd/Graphite Nanofiber	1.7	2-135	0.01	86

## 2.6 Palladium on Carbon

Palladium on carbon (PdC) is an important catalyst in industry for its reduction of organic compound. Palladium on Carbon is a widely utilized catalyst in various industrial chemical processes. It is most typically used in the hydrogenation of aromatic nitro compounds or nitroarenes. In the process of hydrogenation reaction, two hydrogen atoms are added to the double bond of an alkene which results in a saturated alkane. The heat released in this reaction, often referred to as the heat of hydrogenation, is an indicator of a molecule's stability. These hydrogenation reactions cannot occur without the presence of a catalyst even though it is thermodynamically more favorable (Lew, J 2016). Catalysts are required for the reaction to function. Without the presence of a catalyst hydrogenation can only take place in the presence of extremely high temperatures.

Reactions utilizing Pd/C, can reduce alkenes to alkanes in the presence of hydrogen and can also reduce aromatic rings such as benzene. In the reactions shown in the *Figure 4* below Pd/C is used to reduce various multiple bonds such as nitro groups, nitriles, and imines.

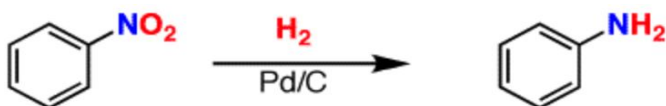


**Figure 4a: Palladium in Presence of Hydrogen Reducing Nitro Groups**

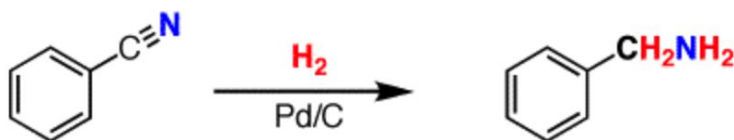


**Figure 4b: Palladium in Presence of Hydrogen Reducing Nitriles**

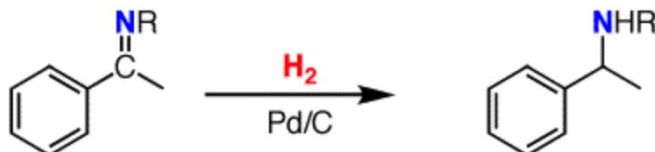


**Figure 4c: Palladium in Presence of Hydrogen Reducing Imines (Taken from James,2018)**

### 2.6.1 Pd/C applications

Paul Sabatier won the 1912 Nobel Prize for discovering hydrogenation. He first used nickel as the catalyst for hydrogenation, however, he later discovered, Palladium, Platinum and Rhodium are the most capable catalysts. In the research, he found that the activity of catalysts are most likely depend on surface area, which brings supported catalysts to the world, and that was the first appearance of Pd/C as a high surface area catalyst. (James, 2018)

As a catalyst, the most common use is for hydrogenation of Alkene. The characteristic of noble metal helps Pd/C absorb hydrogen and alkene onto the metal surface, which provides a environment that fasten the hydrogenation reaction. During the reaction hydrogen and alkene attached to the Pd surface separately, and then one of the hydrogen atom transferred to alkene which detached them from the surface, and as the second hydrogen transferred, the alkene has been fully hydrogenated to a alkane atom, also the atom has been cut loose after this final step, see *Figure 5*. Pd as a noble metal has a character that is strong enough to absorb hydrogen and alkene but not strong enough to keep them on the surface permanently. (Chemistry LibreTexts).

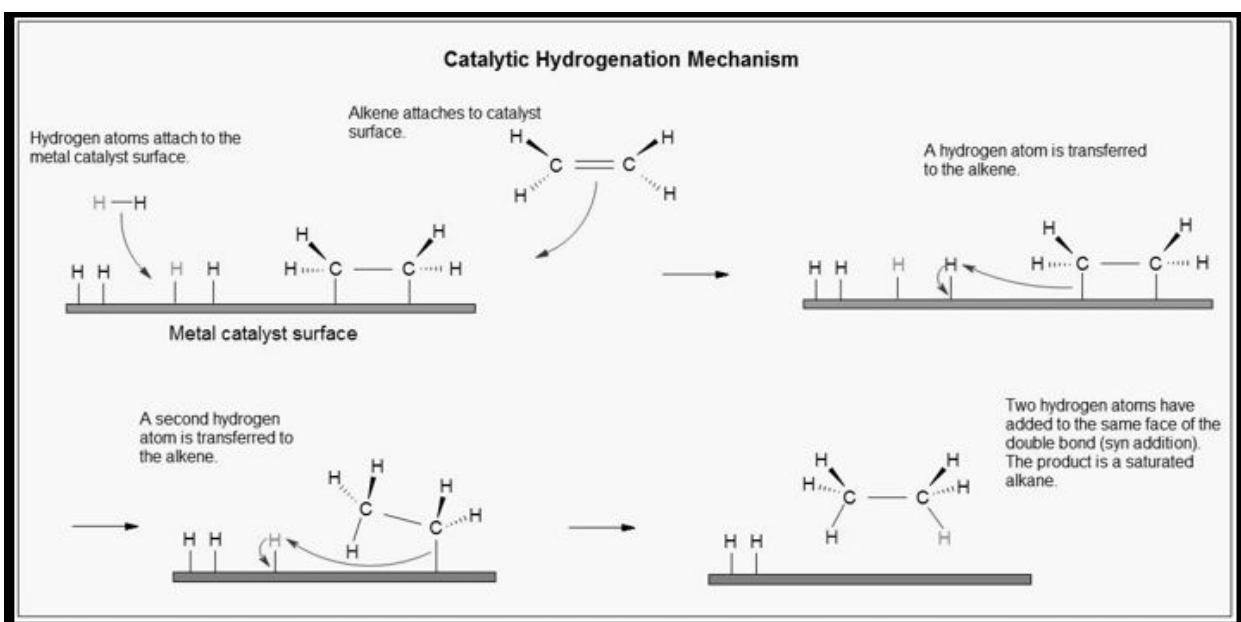


**Figure 5: Schematic of catalytic hydrogenation.** Shows the 1:1 ratio of Hydrogen-Palladium bonding.

## 2.7 Typical Analytical Methods

### 2.7.1 Chemisorption

Chemisorption with Hydrogen or Carbon Monoxide is a common way to determine dispersion of active sites on the catalyst since adsorption is limited to the metal palladium. Chemisorption involves interaction between an electron flexible molecule such as hydrogen and the sp and d orbitals of the metal atom.

$$\begin{aligned} \text{Total Moles Adsorbed (tma)} &= [(peak\ 1 - peak\ avg.) + (peak\ n - peak\ avg.)] * mol\ injected \\ \text{Metal Surface Area} &= (tma/grams\ of\ Pd) * (Pd\ x\ SA) * (6.03 * 10^{-3}) \end{aligned}$$

### 2.7.2 Physisorption

Physisorption on the contrary, involves weak Van der Waals interactions between the entire catalyst and the probe molecule. Brunauer Emmett Teller (BET) analysis utilizes an inert probe molecule such as nitrogen (N<sub>2</sub>) to determine the entire surface area of the catalyst, support structure included. Specific surface area can be calculated from BET, and total pore volumes can be estimated from the quantity of nitrogen adsorbed at a relative pressure (Wagner, 2011). *Figure 6* below shows the BET graph produced as well as the respective pore size graph.

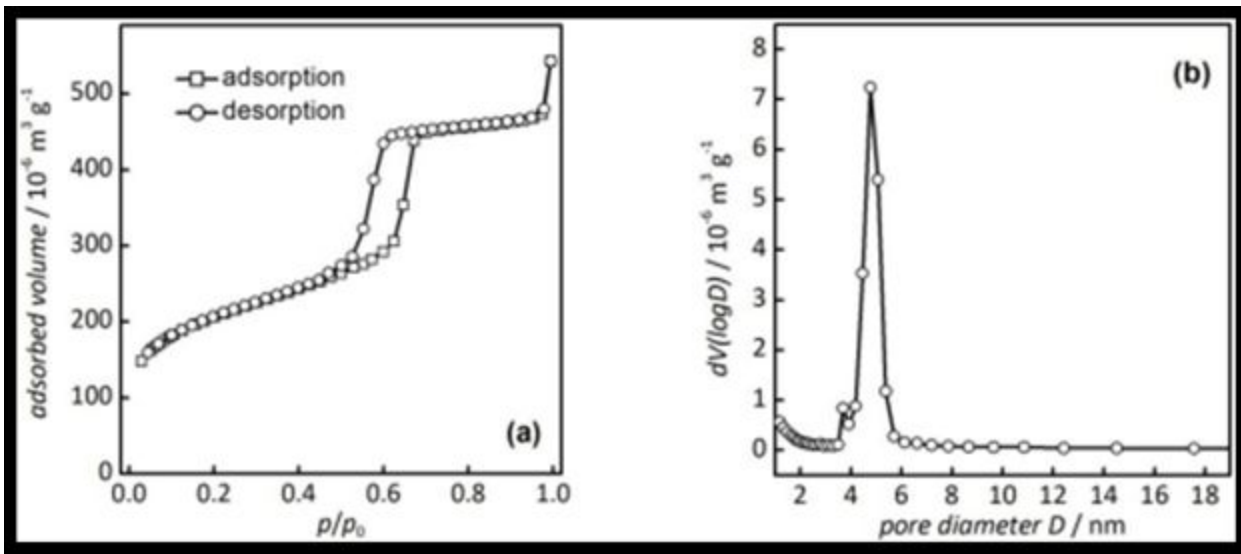


**Figure 6: Comparison of different types of BET graphs. Left-** Physisorption isotherm; **Right-** Pore diameter distribution (Thorsten Wagner, 2011)

### 2.7.3 Temperature-programmed Reduction

Temperature-programmed Reduction, provides a temperature range needed for a complete reduction of the catalyst. With constant flow of diluted hydrogen in an inert stream over the catalyst temperature is ramped, usually around ten kalvin a minute, and the effluent gas content is measured with a thermal conductivity detector. The area under the curve detected is proportional to the total hydrogen consumption expressed as moles of Hydrogen per mol of metal atom used (Amorim & Keane, 2008). See *Figure 7* below for an example of an expected TCD signal on varying carbon supports.

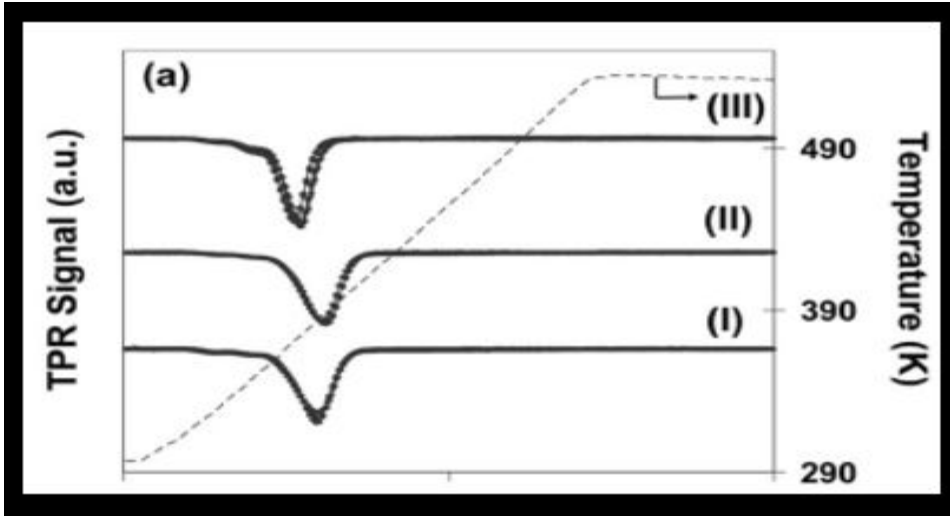


**Figure 7: Comparison of TPR profiles with no support and two types of carbon supports. (I) Bulk PdO, (II) bulk PdO and Activated Carbon, (III) Pd/AC (Amorim & Keane, 2008)**

Utilizing the maximum peak temperature ( $T$ ), and the heating rate  $\beta$  a plot can be made to find the activation energy. Plotting the natural log of  $\beta$  over peak temperature squared on the y-axis, and the inverse of temperature on the x-axis yields the activation energy over the gas constant.

#### 2.7.4 SEM Analysis

Scanning electron micrograph (SEM) analysis is a way to determine the morphology of a surface on a nanometer scale. It can be used to determine leaching of palladium content from the surface of a support. Below are images taken from before and after induced leaching. White particles, matching the SEM images taken of pure palladium powder, can be seen before leaching was induced. After, no particles are apparent. Particle size distribution can also be determined from this method. Based on the equipment at WPI, magnification of up to 10 micrometers can be achieved.

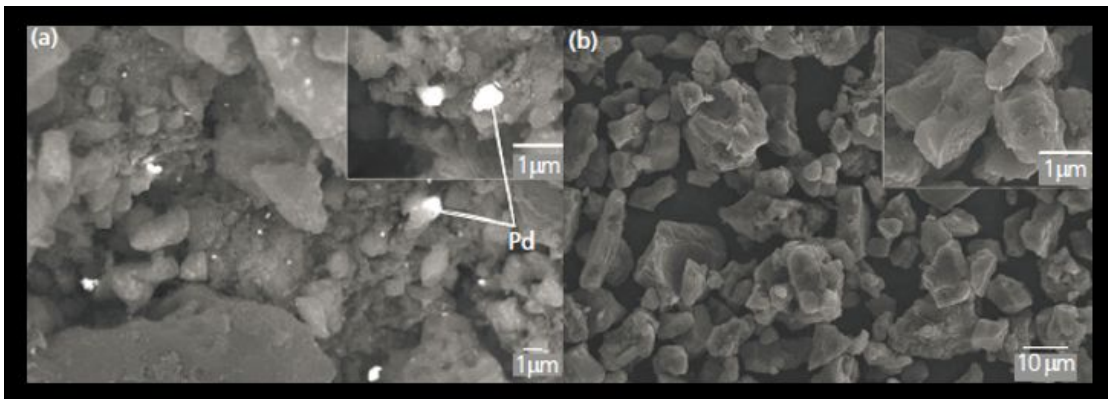


**Figure 8:** **Left**, SEM analysis of Pd/AC before induced leaching - white particles are confirmed to be palladium via XRD analysis; **Right**, SEM analysis of Pd/AC after induced leaching (Sarioglan, 2013).

### 2.7.5 TEM Analysis

Transmission electron micrograph (TEM) analysis is a common investigation technique to determine the changes that occur on the surface of a catalyst before and after testing. Such changes that occur include sintering or change in particle distribution, and leaching. Magnification is typically on the scale of nanometers, as shown below on an images taken from a Heck reaction of bromobenzene with styrene catalyzed by Pd on activated carbon. The carbon particles agglomerate into clumps after the reaction took place. The catalyst was washed with methylene chloride and water, a common procedure used to separate out organic compounds and reducing agents.

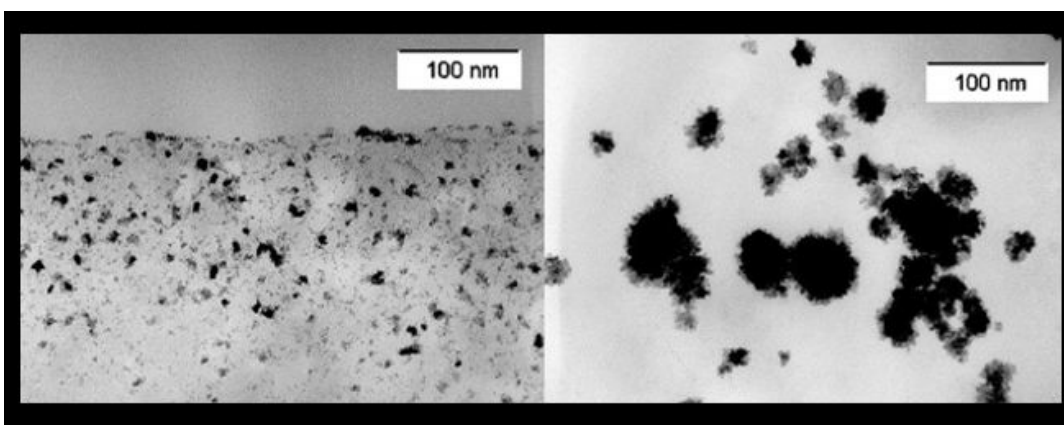


**Figure 9:** **Left**, TEM analysis of Pd/AC before Heck - large surface area due to small particle size; **Right** TEM analysis after Heck reaction - loss of surface area resulting in less catalytic activity (Heidenreich 2001).

### 2.7.8 XRD Analysis

X-ray Diffraction (XRD) analysis utilizes radiation and the resulting angles of the diffracted rays which can be read and used to determine the sample purity of crystalline material. Sample purity is the main focus in determining leaching since a known content amount of palladium is desired. Below are images of an XRD analysis of Pd on activated carbon induced leaching experiment.

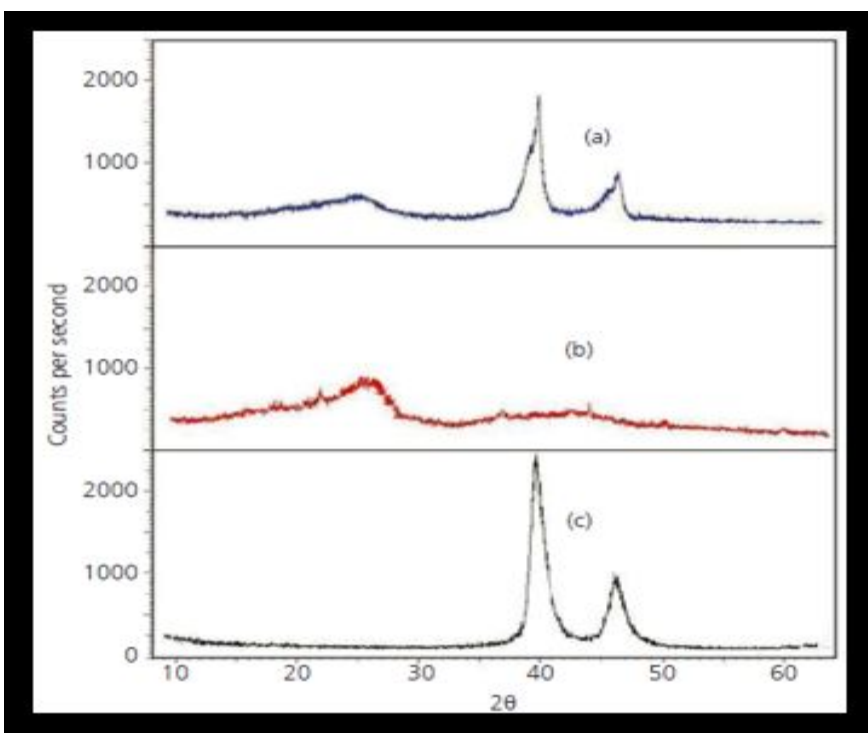


**Figure 10: Comparison of XRD analysis for different state of Palladium on activated Carbon (a) before leaching, (b) after leaching, (c) pure palladium powder recovered (Sarioglan, 2013).**

Lattice spacing can be derived by using the Bragg equation:

$$n * \lambda = 2d * \sin(\theta)$$

Where:

Lambda = Wavelength of the X-rays.

D = The distance between two adjacent lattice planes.

Theta = The incoming angle of X-rays to the normal and reflecting lattice plane.

N = The order of reflection (an integer).

Based on the Bragg equation, the bond angle found via the XRD graph can be verified to be correct. The sharper the peaks are, also conclude information about the diffraction lines which are narrow with perfect crystals (Chorkendorff. Pg. 131-133). Thus the broader the peak, for example part (b) of *Figure 11*, describes a poorly formed crystal, where a narrower peak, such as either part (a) or (c), provide evidence that the crystal structure is better formed. The XRD figure shows that the leaching effect on the catalyst has deformed the crystal structure providing information on the disorientation of the spent catalyst.

### 2.7.9 X-Ray Photoelectron Spectroscopy (XPS)

X-Ray Photoelectron Spectroscopy (XPS) allows for the collection of the elemental composition and the oxidation state of the elements. Atoms absorb a photon of energy such that their valence electron with a certain amount of binding energy is ejected with kinetic energy.

$$E_k = h\nu - E_b - \Psi$$

$E_k$  = Kinetic energy of the electron.

[eV]

$h\nu$  = Planck's constant times the exciting radiation frequency.

[eV]

$E_b$  = Binding energy of the photoelectron.

[eV]

$\Psi$  = Work function of the spectrometer.

The kinetic energy is converted to binding energy. Peaks shown on a graph of the photoemission intensity versus the binding energy can be referenced by consulting binding energy tables. An example of an XPS graph can be seen below.

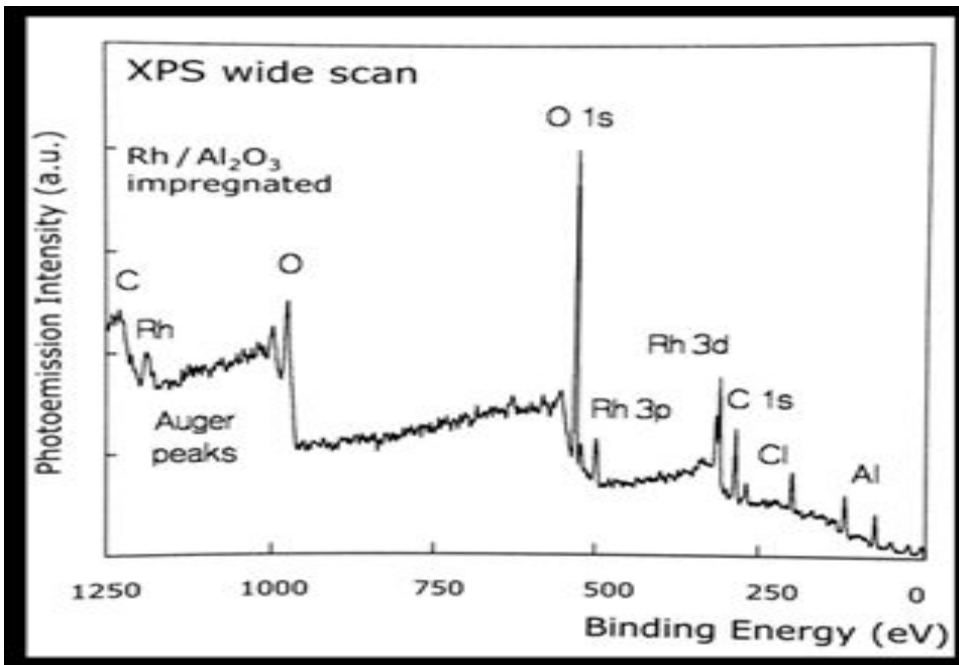


Figure 11: XPS scan of a Rhodium catalyst. Taken from (Chorkendorff. Pg. 136)

XPS also serves as an alternative for determining the dispersion of metal on a supported catalyst. Due to its sensitivity, the ratio of sensitivity of metal atoms to support can be used with different mathematical models in order to determine dispersion. Given the ability of XPS to determine the element concentration, oxidation state, and dispersion it is understandable to why this technique is widely used (Chorkendorff. 134-139).

### 2.7.10 Diffuse Reflection Infrared Spectroscopy (DRIFTS)

Diffuse Reflection Infrared Spectroscopy (DRIFTS), is an in situ method – allowing for data acquisition of heterogeneous catalysts over the course of a reaction. DRIFTS uses complex radiation that can be compared to a transmission spectrum, and offers more data than an Infrared Spectroscopy (IR). Due to more data, DRIFTS can also be used for heterogeneous catalyst which may be hard for alternative methods to be used effectively, such as hydrated samples and certain types of structures. It must also be

noted that DRIFTS is sensitive many conditions during a reaction and a strict method must be followed to ensure readable data. Since there is not a direct relation between the radiation and transmission spectrum, the Kubelka-Munk equation is utilized to produce a result of a spectrum resembling the transmission spectrum (T. Armaroli, 2004). The *Figure 12* below shows the relation between the two:

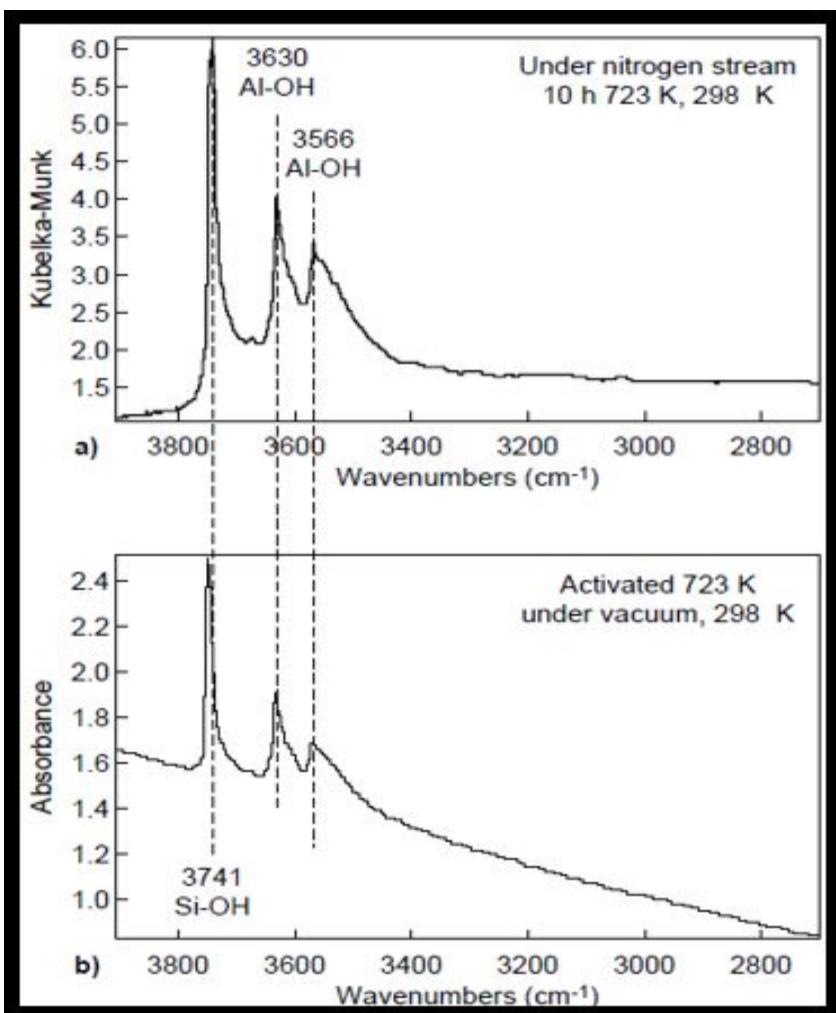


**Figure 12: Top:** DRIFTS radiation spectrum after Kubelka-Munk conversion; **Bottom:** IR transmission spectrum of an identical sample (T. Armaroli, 2004).

### 2.7.11 Inductively Coupled Plasma Spectroscopy (ISP)

Inductively Coupled Plasma Mass Spectroscopy (ICP or ICP-MS) is used to determine the elemental composition with the added capability to obtain isotopic information.

Elements in the sample are converted to ions via Arogn ICP plasma. ICP allows for atomic spectroscopy, and atomic emission spectroscopy. ICP also has an instrumental detection limit for each element which allows for the ability to determine what elements are present (Wolf, 2013)

### 2.7.12 Zero Length Column Technique (ZLC)

The ZLC method is based on the simplification of a catalytic chamber. The chamber is designed to hold a monolayer, allowing for simplification of analysis techniques. This method is typically used in measuring limiting diffusivities for hydrocarbons and other simple molecules in zeolites. Adsorption adsorption in the cell can be considered as a perfectly mixed isothermal, continuous-flow. Originally this method was used by injecting hydrocarbon sorbates, at pressures set so Henry's Law was valid, with high flow for fast heat and mass transfer and limiting the system to very low concentration of sorbate on the surface (Eic and Ruthvan).

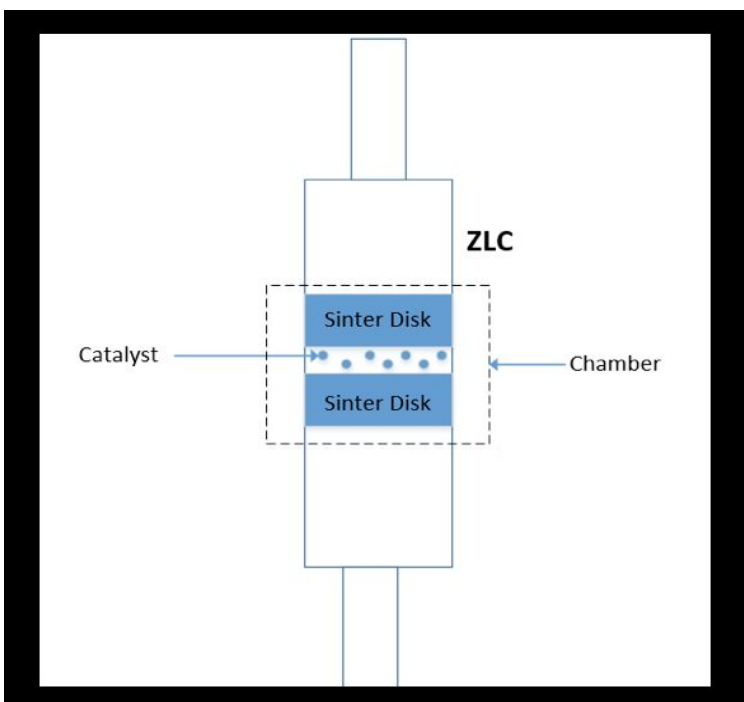


Figure 13: Schematic of the ZLC and Chamber

## 3. Methods

### 3.1 Calibration

This section is the procedure of our calibration of the system for the titration experimental set up. In order to maintain experimental accuracy of the data obtained from our Gas Chromatography (GC) instrument, it was necessary to calibrate the sample loop, so that the molar amount injected was known.

We first utilized the front inlet injector and an gastight injection syringe to create an averaged calibration curve from 50 microliters to 250 microliters. From the data of the first trial, it is evident we can see that the Y-axis value changes as we vary the injection value is varied, see *Figure 14*.

After, we left the titration loop open to the atmosphere and rotated the valve to inject loop volume amounts of air at standard pressure. The amount from titration loop injection was around 470 microliters +\_20, which was outside of our calibration curve. We then used a syringe with injection amounts up to 1000 microliters.

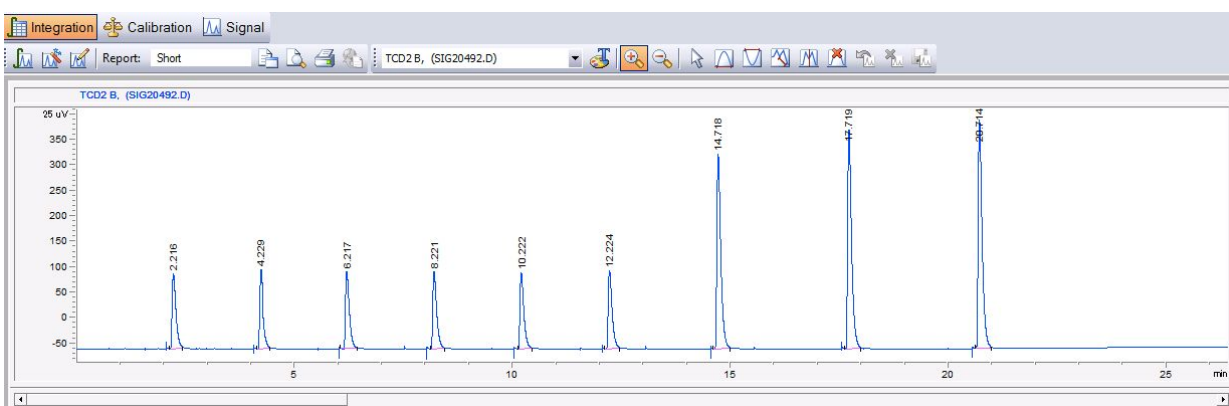


**Figure 14:** Calibration data of injection using front inlet.

Initially, an injection volume of 200 uL was injected and produced a peak area response of approximately 170 ppm which matched the previous calibration run. Four trials of injection with 400, 600, 800 and 1000 uL respectively were done and showed a proportional increasing trend of peak area, see *Figure 15*. For increased accuracy the four trials were repeated three times in order to get the average peak area.

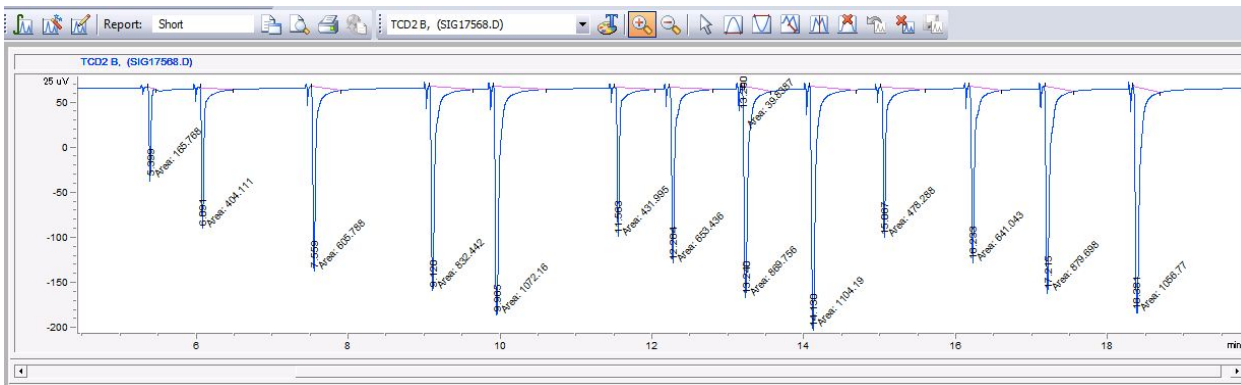


**Figure 15:** Data of injection using front inlet with higher injection volume.

As we analyzed a proportional relationship between injection volume and peak area, we made a plot with peak area as x-axis and injection volume as y-axis, see *Figure 16*. The reason for the distribution of the axis is based on the desired sample loop volume and the response from detector which will show the known peak area.

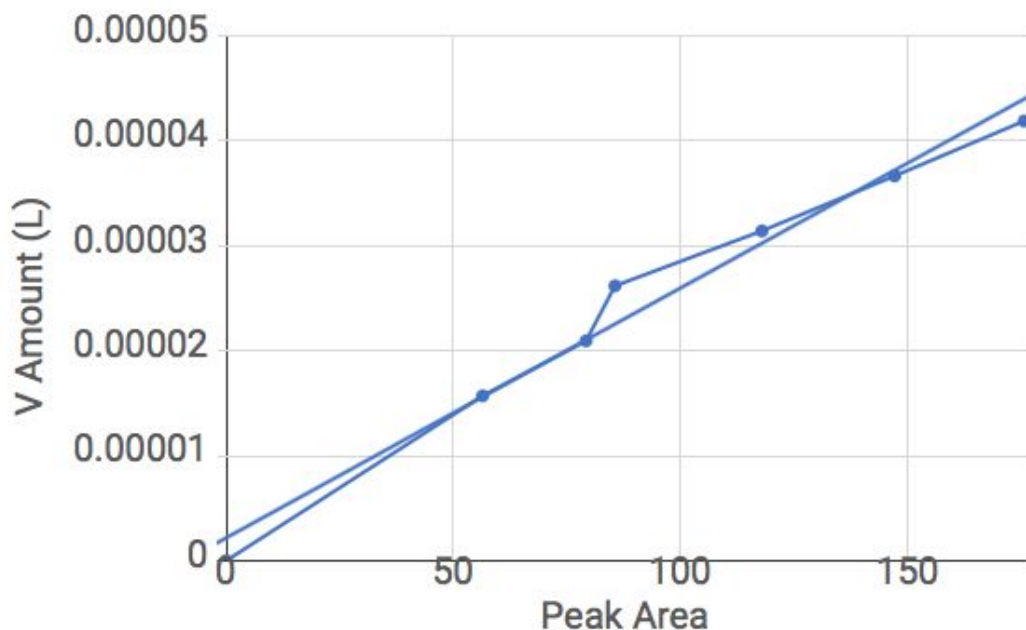


**Figure 16:** Calibration curve of Pulse Titration

he trendline is linear so we can get the slope of the line and simply average the five peak areas of all trials by manual injection. From the data we get from the TCD on the GC, the average peak area was 469.63 ppm, and times the slope we get a volume of 422.66  $\mu\text{m}$ . Since titration loops come in standard sizes, we made the assumption that our titration loop is in fact 500  $\mu\text{m}$ . From this we then converted the volume amount to moles and used this number in our calculations, as well as the molar amount of hydrogen present in the mixed stream.

## 3.2 Pulse Titration

### 3.2.1 Equipment Setup

Titration was used to determine the surface area of Pd available and the amount of dispersion within the Pd sample. An Agilent 6890 Gas Chromatography machine was modified in order to titrate hydrogen onto the Pd sample via a switching valve. A ten port vici valve (1/16<sup>th</sup> inch) fitted with a 500  $\mu\text{mL}$  sample loop was used to inject the adsorbate. Two MKS (type 1179) mass flow controllers (MFC), controlled by a MKS

(model 247C) 4-channel readout auxiliary box, were used to mix the contents of the inlet stream, 32 mL/min of pure Nitrogen, and 3.5 mL/min of 5% Hydrogen in Nitrogen. The purge stream was set to 35 mL/min controlled by the GC front inlet, and plumbed to flow to the zero length column (ZLC) in either valve position. The ZLC is made out of one quarter inch union, inside which two sinter disks with a porosity of 20 microns sandwich a 5 to 10 mg catalyst sample – theory is described in the following subsection. The quarter inch union is stepped down to a 1/16<sup>th</sup> inch on the inlet side, and to a 1/8<sup>th</sup> inch on the outlet side which is then directly connected to the thermal conductivity detector (TCD).

The dilute stream is set to flow through the sample loop to the exhaust in position one of the valve, or flow directly to the exhaust exit once the valve has been switched and the exact amount in the sample loop pushed through to the column by the purge stream. The effluent of the column is immediately directed to the thermal conductivity detector. See schematic below:

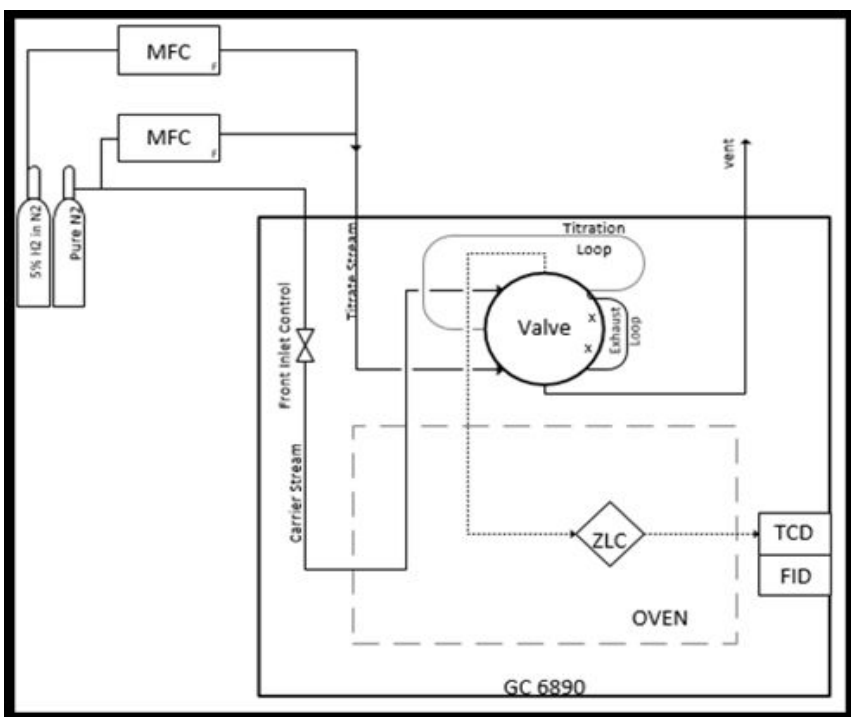


**Figure 17:** System Schematic. Not shown: MKS control box, and computer station.

### 3.1.2 Theory

Zero Length Column (ZLC) chromatography is a well-known way to measure diffusion of a hydrocarbon over a heterogeneous catalyst - typically a zeolite, however, it works equally as well for catalyst titration. The ZLC method allows for the ability to assume the chamber is well mixed, negligible fluid hold up, limited diffusion restrictions, and diffusion only depends on purge rate and equilibrium constant (Duncan & Moller, 2000).

Nitrogen is used as the reference and purge stream, while a dilute (0.45%) hydrogen stream is used as the titration stream. Such a low percentage of Hydrogen is used to prevent saturation until the 4th to 5th injections have been completed. This allows a certain amount of resolution allowing to calculate the exact amount that gets adsorbed per injection as well as the sum adsorbed on the surface at saturation.

The TCD, referenced to Nitrogen, reads the amount of Hydrogen per time which is then manually integrated using Agilent Chemstation software. The total amount of each peak area is quantified in Pico amps seconds, which can be related to the molar amount of Hydrogen through a calibration curve – described in the following subsection. The following equations calculate the surface area of Pd available, as well as the dispersion coefficient. An actual calculation is carried out in Appendix 7.1.

$$R_x = \frac{Ns}{Ab} \quad [\text{mol/pA}] \quad [\text{Eq. 3.1}]$$

$$H_{sum} = \frac{Ns}{ln} \quad [\text{mol}] \quad [\text{Eq. 3.2}]$$

$$Ad_{sum} = H_{sum} - SUM(Pkar) * R_x \quad [\text{mol}] \quad [\text{Eq. 3.3}]$$

$$Atsum = Adsum * 6.022 * 10^{23} \quad [\text{Atoms}] \quad [\text{Eq. 3.4}]$$

$$A = \frac{nm * Xm}{ns} \quad [\text{Pd m}^2] \quad [\text{Eq. 3.5}]$$

Where:

Ns = Amount of hydrogen moles in the sample loop.	[mol]
Ab = Average peak area of saturated signal.	[pA]
Rx = The resonance ratio	[mol/pA]
Hsum = Total amount of hydrogen injected.	[mol]
Adsum = Total amount of hydrogen adsorbed.	[mol]
Atsum = Total amount of hydrogen atoms adsorbed.	[atoms]
Nm = Monolayer adsorbate uptake – H2 atoms on the surface.	[atoms]
Xm = Number of metal atoms associated with adsorbate atoms.	
ns = Number of metal atoms per unit area of metal surface.	[atoms/m <sup>2</sup> ]

After the surface area of palladium is determined, the dispersion amount can now be determined. Total dispersion would mean every palladium atom is dispersed far enough apart where they would not hinder adsorbate uptake from another palladium molecule, and that no support atoms are hindering the adsorbate rate either. Total dispersion would result in a value of 1, where complete agglomeration, and coverage of the palladium surface, would result in a value of 0. An equation for dispersion is given below (Quantachrome Instruments):

$$D = \frac{Vm * S * M}{100 * L} \quad [\text{Eq. 3.6}]$$

Where:

Vm = micromoles per gram derived from the specific volume adsorbed.
S = Stoichiometry of metal to adsorbate.
M = molecular weight of metal
L = Loading percent of metal

This is however, based on the volume amount of hydrogen read through the detector. In our case it is easier to use the molar amount read based on our calibration. An alternative form of dispersion that is used is this:

$$D = \frac{Nm * S}{Npd} \quad \text{[Eq. 3.7]}$$

Where:

Nm = Moles of Hydrogen adsorbed per gram of catalyst

S = Stoichiometry of metal to adsorbate.

Npd = Theoretical molar amount of metal per gram of catalyst.

This provides a ratio of available metal moles per gram participating in adsorbate reactions to the theoretical amount that would be available if the entire molar amount of palladium per gram was available to participate in the reaction. The equation was converted to area units for theoretical and experimental numbers which resulted in the same percentage of dispersion.

### 3.1.3 Procedure

For pulse titration, 5% hydrogen balance nitrogen is mixed with pure nitrogen to achieve a titration flow of 0.5% of hydrogen at 35 mL/min total flow, The GC front inlet was set to 35 mL/min of nitrogen for an equivalent flow in the carrier stream. A Vici 10-port valve was used along with a 500 umL sample loop, and was manually operated for each injection. When testing was underway, a replacement 6-port valve piece was ordered so the system could be later automated with the available GC valve actuator.

Three runs, at each temperature of 40 C, 80 C, and 120 C were selected for the titration runs in order to generate a broad range of temperature data. A blank chamber with two sinter disks ( 20 micron porosity) was used to collect background data. The amount injected per titration was determined by taking the average of the last three peak areas. Each valve switch injection was held for 30 seconds, and each load position was held for fifteen seconds, as no difference in peak area was determined if

the load was held for longer. Runs were also done in tandem with a temperature program desorption (TPD) section where the oven temperature was increased to 250 C at a rate of 10 C per minute and held for two hours. In addition to the TPD method, the temperature ramp desorbs all of adsorbed hydrogen. The TPD method will be discussed later on. Each run follows the same time frame – 50 minutes for titration, two hours at TPD peak temperature, followed by a temperature deramp and 10 minutes at the original temperature to allow a cool down of the GC areas such as the front inlet adjacent to the oven.

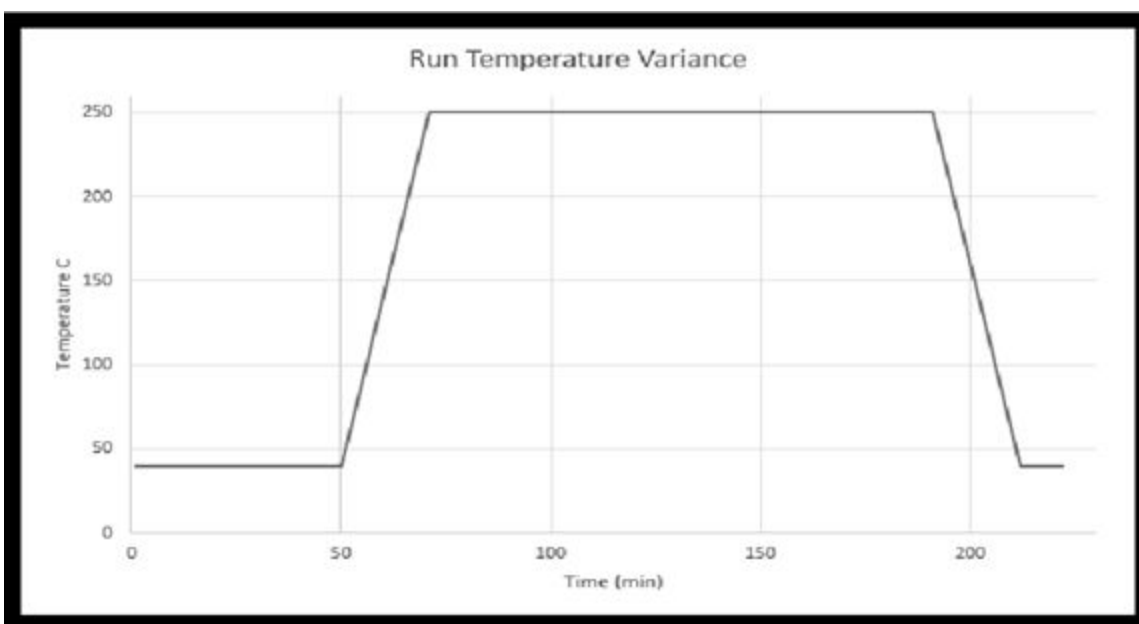


**Figure 18:** A temperature variance outline of a 40 C titration run with TPD.

A test catalyst from ETEK was used in order verify that our system worked by confirming our experiment matched – within reason - the characteristics of a known commercial catalyst. The test catalyst, 20 wt% Palladium on Vulcan XC-72 (activated carbon), was weighed out to a 7 mg sample, which was directly loaded between the sinter disks of an identical ZLC chamber to the blank ZLC used for background data collection. The loaded catalyst was then activated at 250 C for four hours.

One blank run was processed the same day as the first loaded run in order to ensure limited possibility of TCD filament change as the filament is susceptible to oxidation. Loaded commercial catalyst runs were done back to back at each temperature. Having the catalyst loaded in the chamber resulted in a longer period of time for the signal to return to baseline, so it was determined that each injection period lasted four minutes with a 30 second titration loop load time. With 50 minutes per titration cycle, a maximum of ten titrations were done for each run.

Data was recorded and the peak areas were manually integrated using the Agilent Chemstation software. The integration was found from a horizontal bottom line from the lowest point after the valve switch to the valve switch back. Process details of manual integration are further discussed in the *Error Analysis* section. See *figure 19* below for Chemstation example:

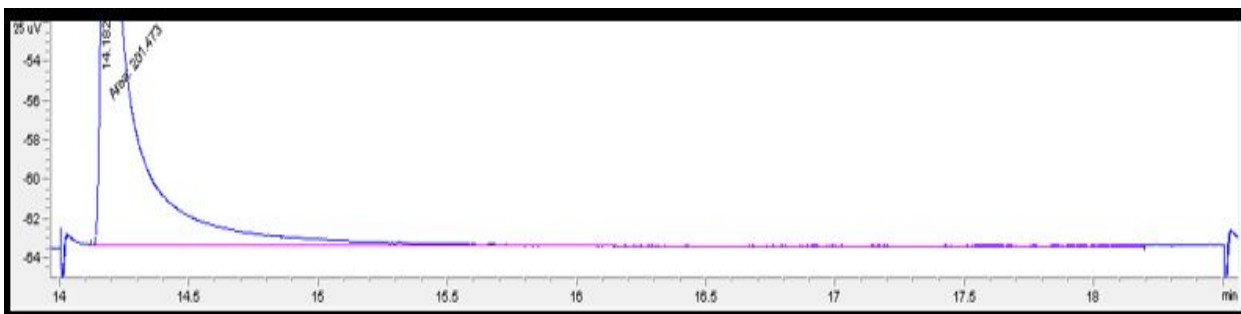


**Figure 19:** Four minute loaded injection at 40 C, with 15 second load.

Confirming literature values with the test catalyst, the switch was then made to the Sunovion catalyst. The catalyst was supplied in four bottles with three separate lot numbers. The bottles were clarified 'fresh' and 'spent'. The catalyst provided was supplied to Sunovion by Degussa Chemicals - a company which is no longer operational by the time these experiments took place.

A identical ZLC column was made in order to allow switching between blank, test, and actual catalysts without having to replace the catalyst in the column for each series of

tests. The fresh catalyst was then activated under the 35 ml/min nitrogen flow at 250 degrees centigrade for four hours. Three sets of ten titrations were then performed at the same three temperatures totaling nine runs. Data was then averaged and plotted as number of titrations versus amount of hydrogen adsorbed.

The certainty of baseline saturation after 10 titrations was unclear as the results continued to adsorb less hydrogen at later injections. As discussed further in the results section, thirty titration runs or three times the original amount, were then employed to further clarify this. The adjusted method procedure will now be discussed.

Due to 10 titrations requiring a total of 50 minutes alone for manual titration, the 6-port valve was then installed using the same 500 uL titration loop with everything else in the system kept identical. To verify that this new valve worked, the test catalyst was reinstalled, activated, and underwent a series of ten titrations to match the 10-port valve data. Having confirmed this, the Sunovion palladium on carbon was reinstalled, reactivated and underwent a new series of 30 titrations followed by an identical temperature ramp after the 30th titration. Due to the chemstation software inability to incorporate more than twenty valve switches, or ten cycles, a new run at the three temperature was written in the software. The setup was to run the new run, 10 titrations, repeated once for titration 11 to 20, followed by the original run with titrations 21 through 30 and the temperature ramp. In doing so, however, the machine had an extra five minutes between the 10th and 11th titration and 20th and 21st titration due to the runs switching on the software.

This new method was performed for the fresh Pd/C three times at each temperature, as well as for the spent Pd/C which was loaded into the old test catalyst ZLC column with new sinter disks after the ZLC was cleaned with isopropanol followed by a washout with deionized water.

## 3.2 Zero Length Column

### 3.2.1 Procedure

The valve configuration was switched from titration to allow constant injection of the 5% hydrogen balance nitrogen and an available purge stream upon valve switch. Injection and purge stream were set to 25 ml/min. Three injection times were tested - 15, 45, and 60 minutes, at which times the system was purged with nitrogen for an hour. Temperature programmed desorption was conducted following each run also allowing the total desorption of hydrogen. The profiles from the valve switch to the signals return to baseline were extracted and analyzed with MatLAB in *Appendix 8.5* to determine the diffusivity.

## 3.3 TPD

Temperature Programmed Desorption is a analysis following each ZLC run for diffusion analysis. After injecting different amount of hydrogen when doing ZLC experiment, hydrogen has been adsorbed onto the surface of Palladium on Carbon catalyst. From research, the hydrogen desorption temperature is above 200 degrees celsius. In order to determine the amount adsorbed, we ramp up the temperature to 240 degrees celsius. On top of the regular linear trend of intensity detected by the Gas Chromatography instrument, there's a peak which is the amount coming off from the catalyst surface. We recorded the surface area and generated a graph of the intensity versus temperature to compare and contrast the amount desorbed from the surface for each run (different amount injected). From the calculation of pulse titration, theoretically the amount desorbed are the same for three runs (15 mins injection, 45 mins injection and 60 mins injection), since 15 mins straight injection amount is exceeded the amount of 30 titrations.

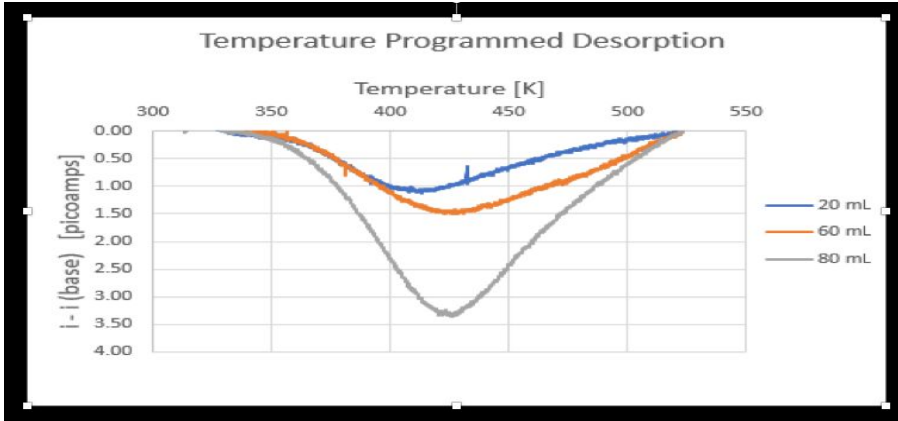


**Figure 20:** Temperature Programmed Desorption date of hydrogen intensity v. system temperature.

### 3.4 SEM

This section of our procedure relates to the SEM procedure. The SEM technology utilized provides a detailed high resolution image of the sample. The scanning electron microscope (SEM) uses a focused beam of high-energy electrons to generate a variety of signals at the surface of solid specimens (Swapp,2017) . In the case of this SEM gold was applied to the Palladium sample to obtain a high resolution image of the sample. of particle counted in the image .

The software ImageJ was utilized to obtain additional information regarding the average particle size of each particle. Rather than utilize the hand measurement method an automated ImageJ was utilized. The scale of the image was set by measuring a straight line in the program according to the known scale of the image in microns. This scale in the program would thereby measure every particle in accordance to the scale of the actual SEM image. The color threshold of the SEM image taken was adjusted to better define the particles in the SEM image. Then each particle was analyzed and measured lengthwise. The reason that each particle was measured lengthwise is due to the graphitic sheets as shown by the images. As a result of the sheets, any target molecule that needed to access the active palladium would need to enter in between the sheets rather than through the top. To determine the percent error of each measurement made by the ImageJ software a chosen particle

was measured lengthwise 10 times to obtain the error of the Image J software. The lengths of the chosen particle was averaged, then the highest and lowest values amongst the ten lengths were used to calculate the percent error. The highest amongst the two was determined to be the percent error of the ImageJ measurement.

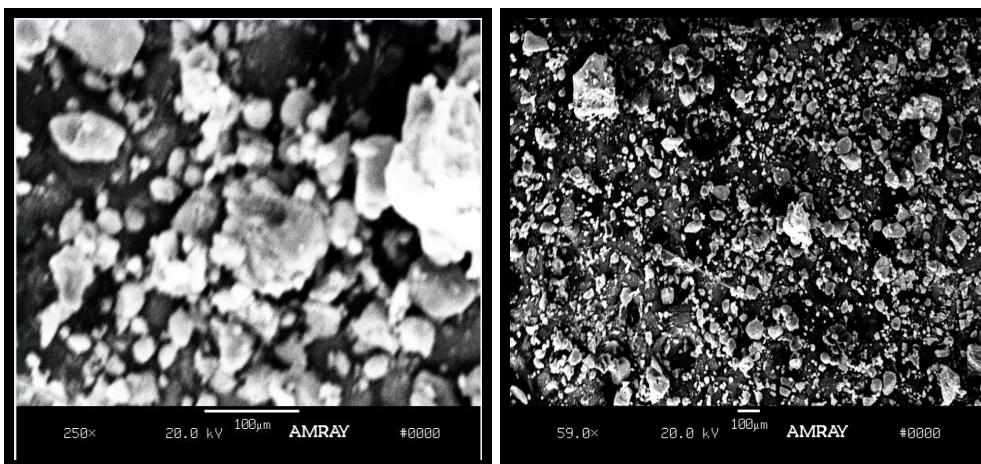


**Figure 21: Left.** SEM image Test Catalyst Palladium on Vulcan XC-72 scan (zoomed). **Right.** SEM image Test Catalyst Palladium on Vulcan XC-72 scan (original)

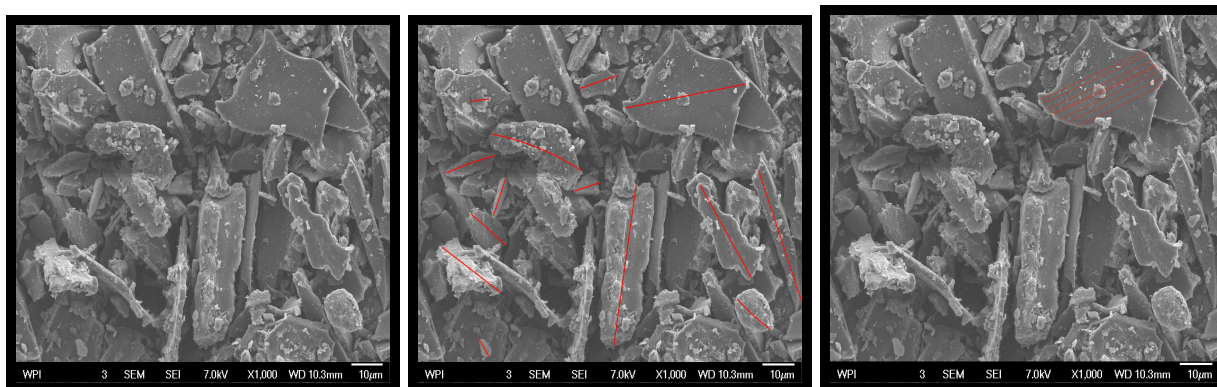


**Figure 22: Left.** SEM image Palladium on Carbon Spent scan 1000x zoom. **Middle.** SEM image Palladium on Carbon Spent scan 1000x zoom( Sample Particles Analyzed with IMAGEJ software for particle lengths). **Right.** SEM image Palladium on Carbon Spent scan 1000x zoom( Particle Analyzed with IMAGEJ software for percent error)

### 3.5 BET

The Brunauer–Emmett–Teller (BET) method was used to analyze the total surface area of the Palladium on Carbon catalyst using an isotherm physisorption instrument that involved no chemical reaction. There are two stages of the process, degassing and analyzing.

Degassing is a process where the temperature is ramped up under vacuum conditions to desorb and vacuum out any impurities such as air and water vapor from the surface of the sample. This process involves 2 hours vacuuming before the temperature ramp to create an isolated system within the glass tube, followed by a 10 to 15 hours ramping from ambient temperature to 300 degrees celsius. A post run with further ramping to 350 degree celsius for half hr has been done to test if there's any more content coming out from the surface. After the post run, the system cools down to ambient temperature automatically.

The glass tube was transferred to the analyzing station in order to determine the actual surface area.. This process required liquid nitrogen in the system. With a P-0 tube testing with the sample simultaneously, the pressure in the P-0 tube was used as a reference pressure to determine the volume of sample tube. Dosing the nitrogen, there were pressure changes within the sample tube, the system would record the partial pressure scaled 0 to 1 inside the sample tube by using the detector. As more nitrogen was dosing into the system, the partial pressure got closer to 1 and finally stopped. The system would generate a graph using partial pressure as the x-axis and amount adsorbed as y-axis. B.E.T analysis involves taking the middle section when partial pressure is from 0.05 to 0.5. The reason of taking only middle section is that this is the region that nitrogen is forming a monolayer on top of the sample surface. From the image below, we can see there are three stages, the first one is when nitrogen filling the pores, and second stage is when nitrogen forming the first layer, which is

known as monolayer on the surface, and the third stage is when nitrogen forms a multilayer. See *Figure 22* for a sample BET graph.

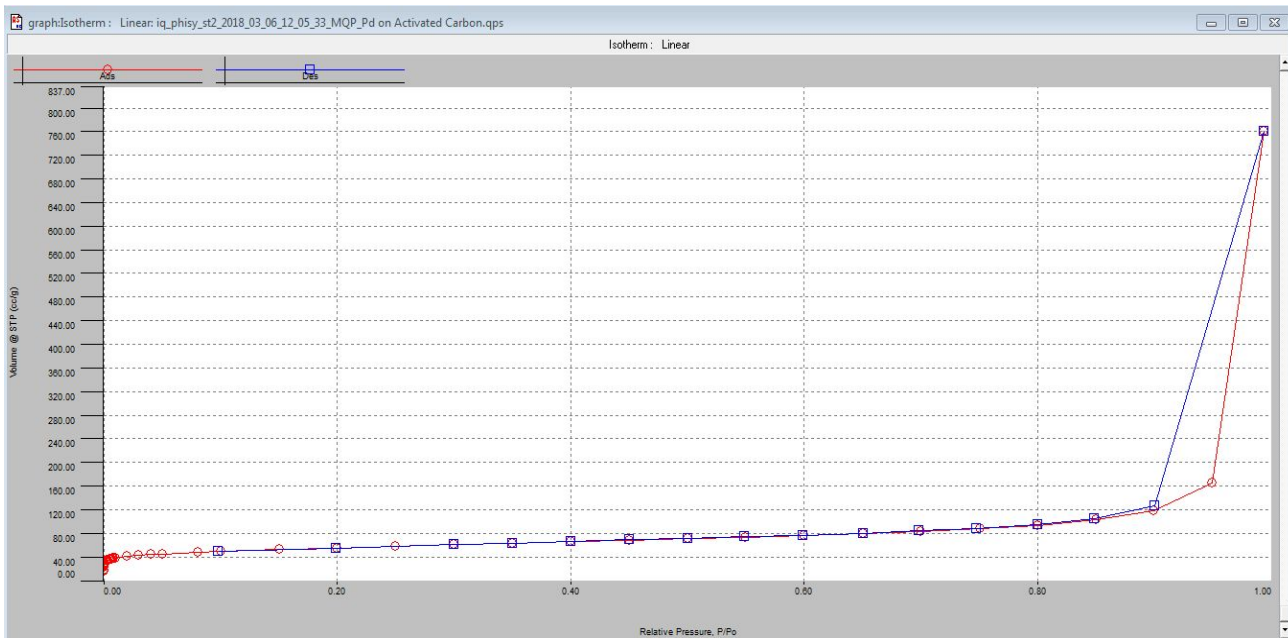


**Figure 23:** Sample BET analysis graph of test catalyst. Y-axis is amount of nitrogen physisorbed, X-axis is the partial pressure of the system.

After the determination of test catalyst there were some issues within the Quantachrome Autosorb system. The system failed the test of void volume and failed the leak test for two times. We used another sample that requires a shorter time for each run to check system error. The result of test was negative. A further test run has been done with a system failure 30 minutes after the run started. Due to this system failure, we were not able to collect data on the total surface area of the Sunovion catalyst.

### 3.6 Safety

The safety data sheet states the 10 wt.% Palladium on Carbon is stable under the recommended storage conditions being sealed and wetted. This palladium on carbon,

specifically, contains 50 percent water for safety purposes. There is a prevalent safety and health risk when running this system as reagents such as Pd/C are extremely flammable and can ignite solvents and hydrogen. Extra caution must be taken when in the presence of hydrogen gas especially in the presence of pyrophoric material. The Gas Chromatography instrument heats up to temperatures well above the ignition point of the catalyst. To prevent the dried Pd/C being exposed to air when the system is being changed or configured, a prevention safety system was installed.

The safety system is what is known as a bubbler which functions through vapor liquid equilibrium with the contained liquid contents being water. The bubbler installed in our system has a small pipe installed through the middle which flows inert nitrogen into the water in bubbler. As the nitrogen gas makes contact with the water, the water vapor then gets carried away by the nitrogen stream exiting the bubbler. The bubbling of nitrogen through the water creates a mixing action more favorable for a higher concentration of water vapor in the effluent stream. The water vapor is then carried through the system into the ZLC chamber and wets the Pd/C allowing for safe exposure to air, even at higher temperatures. The water bubbler vessel schematic is shown below.

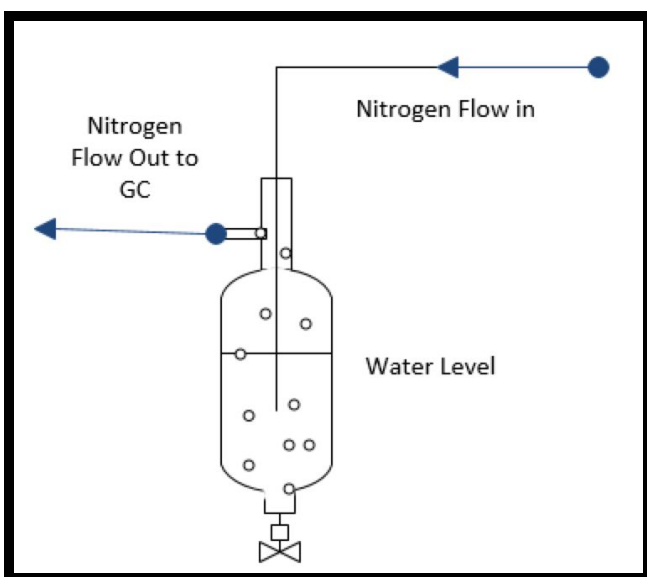


**Figure 24:** Schematic of Bubbler System for system safety.

## 4. Results

### 4.1 SEM

The particle sizes for each of the SEM images was determined by measuring the lengths of each particle for both the fresh and spent particles. According to the IMAGEJ software the average particle length for the Palladium on Carbon fresh catalyst was 6.043  $\mu\text{m}$ , and 7.314  $\mu\text{m}$  for the spent catalyst. The percent error was calculated to be  $\pm 12.49$  percent, by using the software to calculate the same length multiple times. Lengths used for the calculation can be found in the SEM section of the Appendix. See *Figure 25* . part C for image. The images used to calculate the average particle length are shown below.

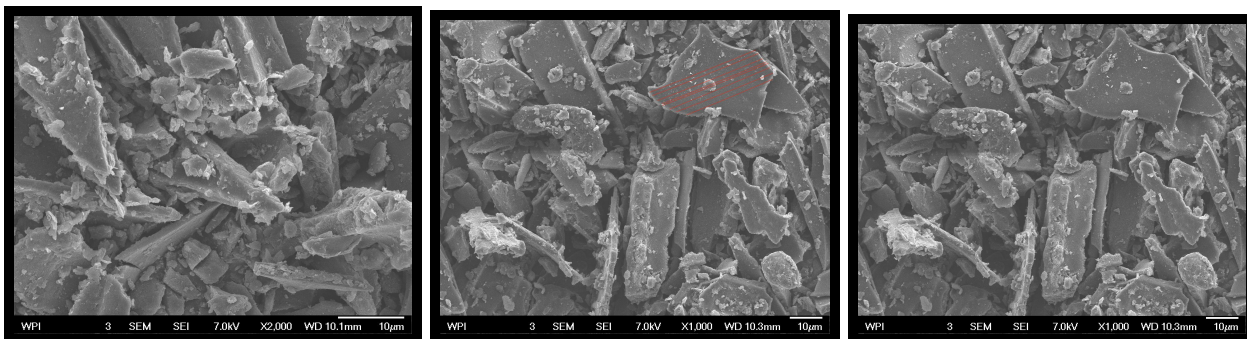


**Figure 25:** **Left.** Palladium On Carbon Fresh Catalyst **Middle.** Palladium On Spent Catalyst( Particle Lengths Analyzed With ImageJ ) **Right.** SEM image Palladium on Carbon Spent scan 1000x zoom( Particle Analyzed with IMAGEJ software for percent error)

### 4.2 Pulse Titration

#### 4.2.1 Molar Amount of Hydrogen Adsorbed

The total molar number of hydrogen was determined for each run done utilizing equation 3.1-3.3. Calculation excerpt can be found in appendix 7.1. The theoretical

injection amount was determined by the last three titrations of each 30 titration run, before the same three temperature runs were averaged and plotted on the graph below. This theoretical amount injected per titration was used when determining the surface area and dispersion discussed in the following section. The following graphs in order cover: the fresh catalyst adsorption, spent catalyst adsorption, and fresh catalyst adsorption with different times of injection.

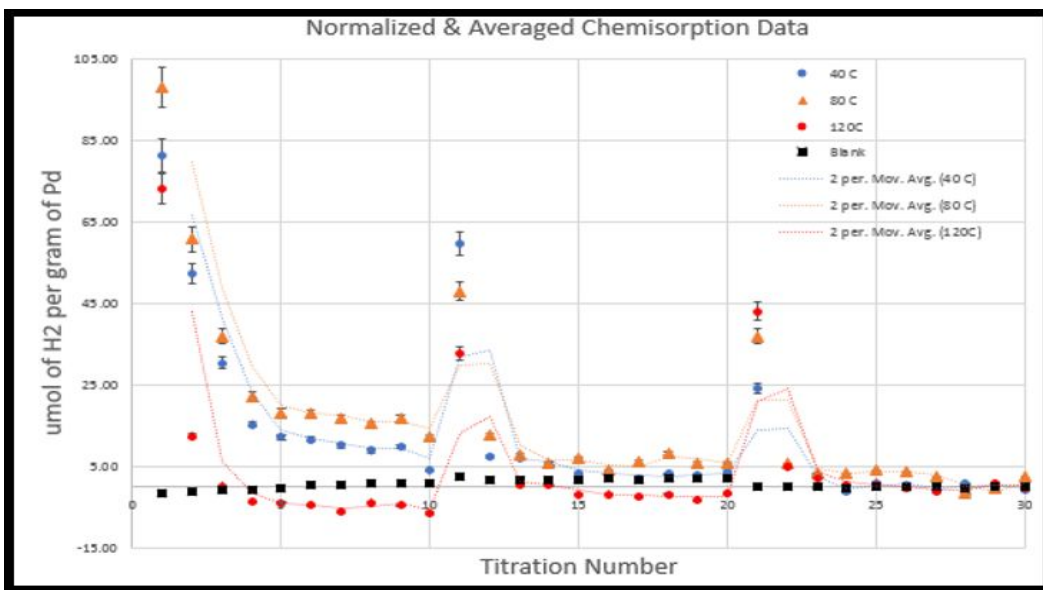


**Figure 26:** Micro-Mol of hydrogen adsorbed at three temperature sets with an error of  $\pm 5\%$ . The two period moving averages are included for ease of following each run's trend. A blank run is included to show that the discrepancies in catalyst runs are not due the detector zeroing or baseline shift.

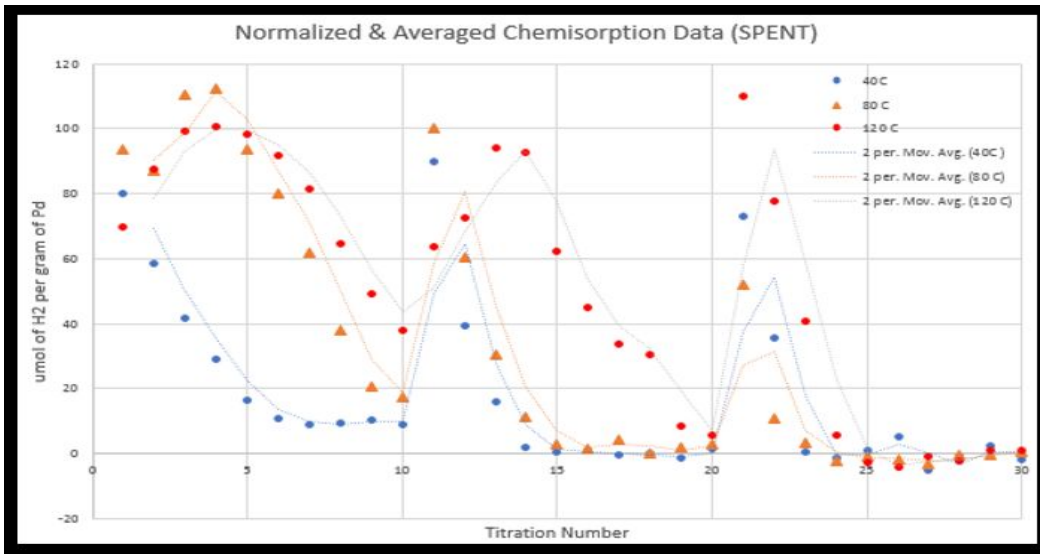


**Figure 27:** Micro-Mol of hydrogen adsorbed at three temperature sets with an error of +/-5%. The two period moving averages are included for ease of following each run's trend.

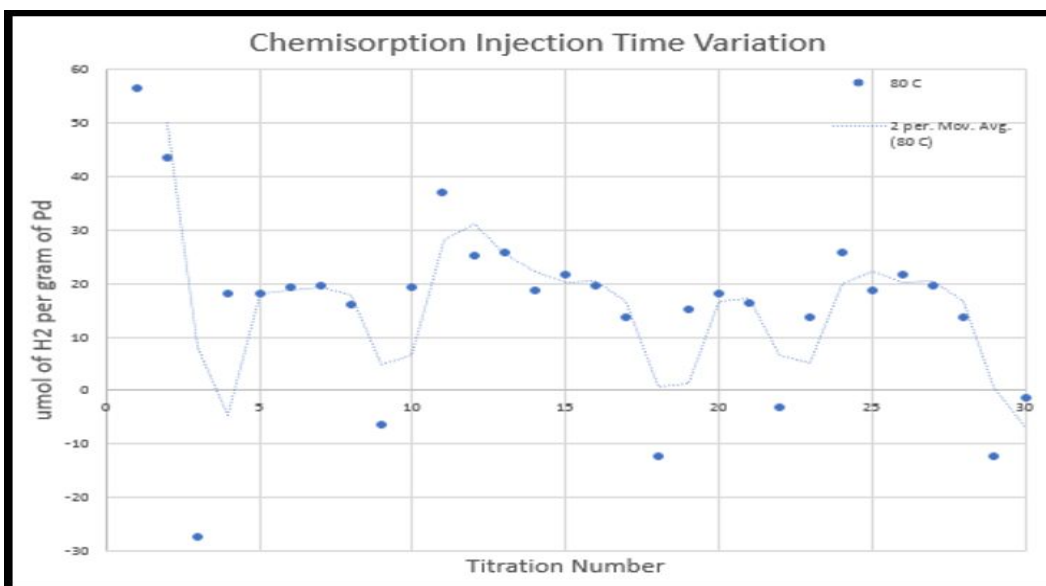


**Figure 28:** Micro-Mol of hydrogen adsorbed at 80 C error of +/-5%. Data is from one single run and not averaged. Injection time varied from titration one to ten and repeated after every tenth titration after. The two period moving average are included for ease of following each run's trend.

#### 4.2.2 Surface Area and Dispersion

The surface area was determined using equations 3.4 and 3.5. The resulting surface area for each temperature set is given in the *Table 4* below.

**Table 4:** Comparison of Sunovion Literature and experimental results. 80 C\*\* Is run performed with the fresh catalyst at different injection times.

<b>Surface Area and Dispersion Comparison Table</b>				
<b>Lot # 51014835 (Fresh Catalyst)</b>				
	Pd m <sup>2</sup> / gram catalyst	Error (m <sup>2</sup> )	Dispersion %	Error
Sunovion	N/A	N/A	N/A	N/A
Experiment 40C	17.1	+ <sub>-</sub> 0.86	38.46	+ <sub>-</sub> 5 %
Experiment 80C	23	+ <sub>-</sub> 1.2	51.59	+ <sub>-</sub> 5%
Experiment 120C	5.8	+ <sub>-</sub> 0.30	13.12	+ <sub>-</sub> 5%
Experiment 80C**	22.4	+ <sub>-</sub> 1.12	50.30%	+ <sub>-</sub> 5%
<b>Lot # 510x4 (Spent Catalyst)</b>				
	Pd m <sup>2</sup> / gram catalyst	Error (m <sup>2</sup> )	Dispersion %	Error
Sunovion	12.9	+ <sub>-</sub> 2.3	29.17	+ <sub>-</sub> 5%
Experiment 40C	25.3	+ <sub>-</sub> 1.3	56.69	+ <sub>-</sub> 5
Experiment 80C	46.9	+ <sub>-</sub> 2.3	105.35	+ <sub>-</sub> 5%
Experiment 120C	71.9	+ <sub>-</sub> 3.6	161.45	+ <sub>-</sub> 5%
<b>Lot # 5106463 (Fresh Catalyst)</b>				
	Pd m <sup>2</sup> / gram catalyst	Error (m <sup>2</sup> )	Dispersion %	Error
Sunovion	27.32	+ <sub>-</sub> 5.1	61.33	+ <sub>-</sub> 11.4

### 4.3 ZLC

Diffusivities for the different amounts of adsorbate hydrogen injected can be seen in the *Table 5* below. *Figure 29* below shows an excerpt of the MatLAB analysis at the time of purge for each run. The exact MatLAB file can be found in Appendix X . C.

**Table 5:** The average diffusivity of each run, along with the beta value for each.

	TPD 15	TPD 45	TPD 60
Diffusivity (cm <sup>2</sup> /s)	5.14e-07	4.82e-07	4.64e-07
Beta Value	2.03	2.03	2.03

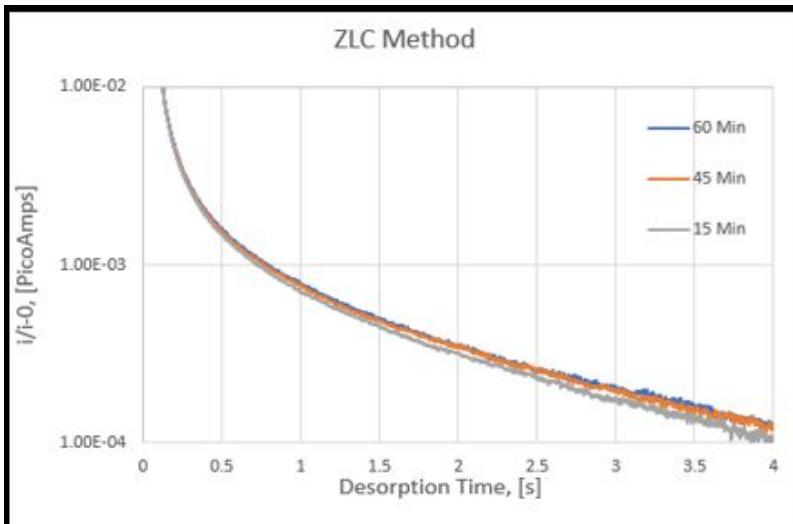


**Figure 29:** Shows the raw data analyzed by the matLAB script. The data present is overlaid for the three injection amounts. The linear region for each was analyzed individually, detailed in the *Methodology* section.

#### 4.4 TPD

The graph in *figure 30* below, was generated showing three different profiles. Each profile is based on the amount desorbed for that specific run. The graph also shows at what temperature range the hydrogen desorbs.

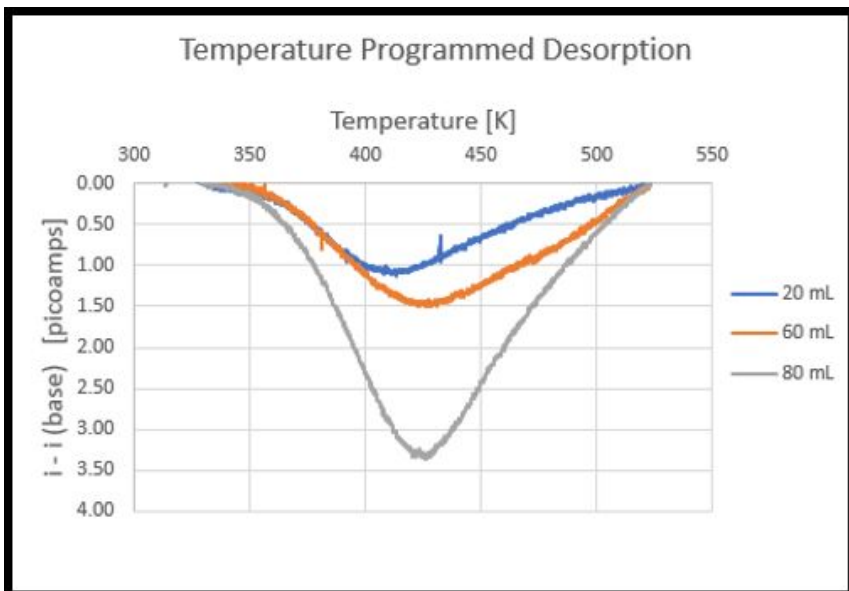


**Figure 30:** Temperature programmed desorption profiles for three injection amounts at 80 C. Injection times are: blue - 15 minutes, orange - 45 minutes, grey - 60 minutes.

## 5. Discussion

### 5.1 Mass Diffusion Limitation

The pictures taken by the scanning electron microscope proved that there is a presence of graphitic sheets in the Palladium on Carbon samples in both fresh and spent samples. The graphite sheets act like stacked pieces of paper in which the only means for entry is within the side of the stacked structure as the target molecules cannot enter through the top thus the graphitic carbon structure poses a problem for accessing the active palladium within the microporous carbon support structures.

During our chemisorption runs it was seen that there was a discrepancy with the expected results - namely the 11th and 21st titration during the fresh runs and the two higher temperature runs for the spent catalyst. The first ten titrations behaved expectedly, reaching close to the baseline value around titration four. The amount adsorbed increased from 40 C to 80 C, then decreased drastically at 120 C. This possibly shows that the chemical bond interactions of hydrogen and palladium are most favorable around 80 C, but possibly get too much energy supplied at higher temperatures around 120 to be favorable. The amount adsorbed at titration 11 and 21 increased drastically for each experimental run. Blank runs were introduced to prove that this was not due to the equipment, but was in fact due to the catalyst. After verifying this, a hypothesis was formed that there is possible mass diffusion limitation in the system, having prior knowledge from SEM analysis.

The spent palladium on carbon was analyzed next, see *Figure 26*. The resulting adsorption amount increased for 80 and 120 C runs contrary to expectation. The 40 C run did not have this, possibly due to the lower kinetic energy supplied to the system through temperature. The unusual adsorption increase from titration one to four added additional indications to our hypothesis. Qualitatively, the difference between fresh and

spent typically means that the palladium metal sinters to a certain extent, and the carbon support is possibly affected to some degree although inert due to likely strain and stress underwent in the previous reaction system. What this means is that there is likely a difference between fresh and spent in how easily the adsorbate hydrogen and nitrogen can flow. This physical change can possibly explain the difference in the adsorption uptake between fresh and spent catalyst. For the spent 40 C, however, this was not seen. The most obvious possible explanation if this is the difference in the kinetic energy present in the system between the runs. This may have factored into the ability for hydrogen to adsorb and behave similarly to the fresh runs despite the catalysts physical change. The spent catalyst adsorption is seemingly more 'sensitive' to temperature. It should be noted, however, that only the 40 C runs for the spent catalyst were averaged, the 80 C and 120 C runs were only tested once so repeatability is not confirmed with the detector device although the 40 C run was done right after. So, further testing is recommended on the spent catalyst with the system to verify the results at the higher temperatures.

Regardless of the different amounts injected, theoretically the diffusivity of hydrogen should be the same since the monolayer amount loaded into the column should be saturated almost immediately and the later hydrogen flowing through the system should just flow through. The experimental results were contrary to the above theory, and confirmed our hypothesis expectations. The diffusivities shown in *table 5* decrease with the amount that is injected meaning that there is more adsorbed onto the surface of palladium due to the diffusion profile changes.

Moreover, higher amounts of hydrogen desorbed from the catalyst for the longer injection run time, which shows that more hydrogen has been adsorbed from ZLC experiment when we extend the injection time. See *Figure 13* for reference. For the zero length column configuration, we are analyzing a palladium on carbon monolayer which makes the required amount of catalyst for hydrogen to saturate limited to a small amount in theory. This, however, is not the case as the TPD profile of our data is not

an overlapping trend which means that there is probable mass diffusion limitation of the adsorbing hydrogen.

Knowing that there are graphitic sheets, an adsorption amount which varies based on injection time, decreasing diffusivities, and different desorption profiles we are confident in saying that there is mass diffusion limitation. We attribute this most likely to the graphite sheets and their microporous structure.

## 5.2 Surface Area Characterization

The fresh Pd/C sample Sunovion literature values matched our experimental results for the averaged 80 C run. The experimental 40 C run was slightly outside of the error region for the Sunovion literature values. Surface area was also determined while the titration times were varied. This still yielded a result within error to the other 80 C run, see *table 5*. See *Appendix 8.6* for a graph depicting the 80 C fresh run with an injection time variation. It should be noted that the fresh catalyst comparison is being made between different lot numbers, meaning that they were possibly from different orders, possibly received at different times. Yet, it is known that they both were stored under the same conditions. It should also be noted that the analysis technique used in the provided Sunovion literature was done under 36 C as opposed to our three temperature range. The amount adsorbed was also determined in the literature based on the partial pressure and volume of hydrogen adsorbed.

The difference in how the two systems operate may have also been a factor in the results. Although our system was tested and confirmed with Pd/Vulcan, mass diffusion limitations were found to be present with our Pd/C likely due to the Pd/C graphite support structure. Such limitations may have affected the fresh catalyst results. Little is known about the literature system setup, however, the sample loaded was 0.06 grams or an order of magnitude more than what was loaded into our sample. If our system,

essentially a monolayer in the ZLC chamber had mass diffusion limitations, it is possible that the literature values had mass diffusion limitations present especially if ten times more was loaded. This possibly explains why the error is so large in the literature values.

The experimental spent catalyst data at the 80 C and 120 C runs are not valid due to the resulted discrepancies seen in *Figure 23*. The 40 C which behaved closer to expectations was double of what was found in the literature values in surface area results. The most probable reason is how our system is set up by titrating a stream through a chamber, which is more sensitive to mass diffusion limitations since our governing analytical equation is a simple mass balance of the adsorbed sum equal to the amount leaving the system subtracted from the amount injected. The literature method of determining adsorption by partial pressure of the system, is not a direct measure of the adsorbate mass of the effluent stream. So, the differences in our 40 C may be possibly explained by this.

### 5.3 Dispersion Characterization

The dispersion of our fresh catalyst again varied by temperature possibly due to bond excitement. Looking at the most favorable 80 C, the dispersion of our experiment was about 52%  $\pm$  5% which is within the lower end of the literature value at 61%  $\pm$  11%.

The non-validity of the spent catalyst experiments at 80 C and 120 C is apparent when looking at the dispersion numbers - both over 100 percent, which is not theoretically possible. The 40 C spent amount was also double of what was seen in literature and roughly within the error of the literature fresh catalyst, contrary to expectations. Based on past dialogue between the catalyst production company Degussa we know that the literature test provided, *“is mainly performed for internal verification that the catalyst activity is within the range we expect. Some customers see a correlation between our activity test and performance of the catalyst in their reaction. Some customers see absolutely no correlation.”*

It is possible that, based on the production of the specific batch and how the catalyst was used, certain amounts of the same lot could be better or worse than the overall average of that lot. In which case we recommend further extensive testing of the same lot, but with a new sample each time. This is something we would have liked to perform, but did not have the time to do so.

## 6. Error Analysis

### 6.1 Pulse Titration

This part of the experiment is constructed with a Gas Chromatography instrument (GC) monitored by two mass flow controllers (MFC) and the data extracted to Chemstation, a PC software that can help us monitor the response of the detectors.

Utilizing the manual integration of Agilent software and a standardized method lead to a small amount of error when determining the peak areas of each titration. The manual integration in figure 31 is done each time from the start of the injection until the valve is switched back. The integration line is manually dragged horizontally from one point to the next. A simple error calculation was done where the end point of the integration was dragged slightly above and slightly below the horizontal axis. The difference between top and bottom from the horizontal line were 6% and 3% respectively. Both percents were added and divided by two to give an average variation of 4.5%. Due to different team members integrating different times, a standardized method was developed to ensure that each run analysis was indeed below 5% error. The point to point integration was done when integrating, then the results were exported to an excel file which extracted the highest and lowest values in the data set, excluding the first four, eleventh, and twenty first data points as they were assumed to vary each time. The difference between the high and low value was then divided by the average of that selected data giving us a percentage which we made sure was under 5% each time

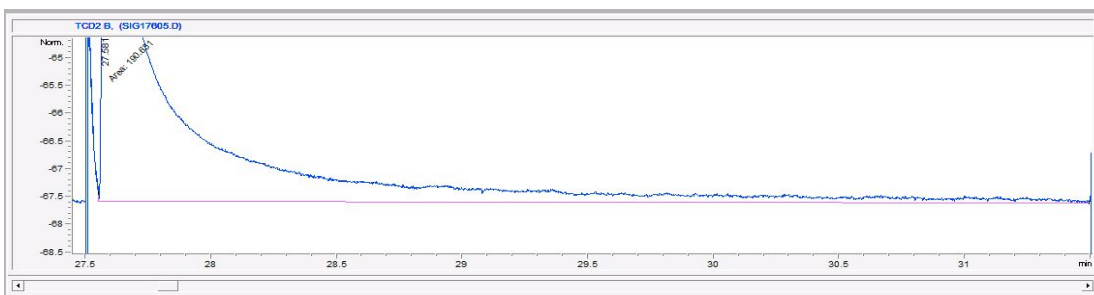


**Figure 31:** Standard way of manual titration for minimizing the error.

For sample loop calibration, the error is most likely from sample loop injection. Inside the GC system, there is pressure on both sides of the valve. When air was injected, the pressure is 1 atm (14.7 Psi) based on the fact that we are manual injecting from atmosphere, however, the other side has a 40 Psi pressure of purge stream. This leads to a fact that no matter how fast we switch the valve there will be small portion of air that gets pushed out of the sample loop which causing the fluctuation of sample loop volume calculation of each run. The first trial lead to a response of 424.97 ppm for peak area while our average peak area is 469.62 ppm with a range from 443.5 ppm to 484.03 ppm. Despide this trial, our average peak area would be more accurate since the error is beyond a 10% acceptable range. When using the manual injector (front inlet of GC) for calibration curve test, the syringe has to poke through a rubber disk that seals the front inlet when it's not being utilized. While injecting, it takes time for purge gas to deliver the inlet gas (air) to the TCD, and during this time of period since the seal is poked by syringe, it's likely to have air getting into the front inlet. Even though the system is designed to seal, we observed that due to the high oven temperature, the seal starts to degrade and no longer perform. We tried to avoid this error by switching to new rubber seal, and verify by monitoring the pressure of the GC at the front inlet. From this we determined that we even had to replace the seal with a new never used seal in order for it not to degrad during the high oven temperature ramps which occur with the experiments performed. The sample loop volume from the calibration is 422.66 um but from the official website of Agilent, the theoretical volume of sample loop is 500 um. This could be error or there are small particles covering the inside wall of the sample loop. By calculating this is 15.5% error, which is beyond tolerance and will affect the result of all calculations. To get around this, we decided to determine the amount injected for each run by assuming saturation and averaging the amount from injection number twenty eight through thirty, the last three injections. Using this gave us a value that is calibrated for each run, also helping us overcome any baseline signal drif the TCD may have between runs.

To equalize the pressure and the flow rate for both sides of valve we used nitrogen as a makeup flow, and dilute the hydrogen at the same time. We set hydrogen flow rate to 3.5 ml/min and makeup flow to 31.5 ml/min to create a 0.5% hydrogen in sample loop. The mass flow controllers are connected to a digital reader with a error of  $\pm 0.01$  ml/min. The minimum flow rate amount two mass flow controllers is 3.5 ml/min, so the maximum error from the digital reader would be on the hydrogen channel. By calculation this is a 2.86% error, so this would be a factor that influences the calculations and the result of project, although it as high as the integration's 5% error.

## 7. Conclusions

The Sunovion Pharmaceutical project goals of characterization and dispersion were completed. The sample of fresh Palladium on Carbon was characterized correctly with chemisorption, and canned electron microscopy (SEM). The spent sample, due to discrepancies over the chemisorption temperature range, we consider to be partially characterized. As discussed in the *Discussion* section, we know that the production company, Degussa, has a variance of reproducibility which may be present within the same lot. Due to this, suggest further testing to confirm the reproducibility with multiple spent samples from the same lot.

Just through SEM, we confirmed that the carbon support consists of graphitic sheets which contain micropores and a selective geometric entrance into the support structure. Due to change in the amount of hydrogen adsorbed during the chemisorption experiments even though saturation should have been reached, and knowing that the carbon support was microporous, the team hypothesized that there were mass diffusion limitations.

The Zero Length Column technique and Temperature Programed desorption were the experiments we introduced to determine the diffusivity and amount adsorbed respectively. The two methods were performed in unison on the device we constructed were performed over a range of molar amounts of hydrogen injected. From this, we determined that there were different diffusivities and amounts adsorbed even after the sample should have been saturated. From these results and the knowledge of the carbon support structure we can conclude that there is mass diffusion limitation. The limitation we also suggest is much more than tolerate, as the limitation was found with hydrogen, a very small molecule especially when compared to the large organic pharmaceutical molecules.

If the goal of Sunovion Pharmaceuticals is to increase mass diffusion of their pharmaceutical molecules through the carbon structure pores based on contingent applications, then we would like to make the following recommendation to Sunovion Pharmaceuticals a carbon support switch from a microporous support structure to a macroporous support structure. Since the palladium present is also similar to a coating, a spherical carbon structure should provide the most surface area. Lastly, we would like to note that there should be further testing to understand the optimal temperature range at which adsorption occurred as seen in our chemisorption experiment.

# 8. Appendix

## 8.1 Titration Calculations

Sample Loop	$N_s := 8.76E-08$ [mol of H2]	$wt := 0.1$ 10%_load
Average Peak Area	$A_b := 160$ [pA]	$Pd_{mw} := 106.42$ $\frac{g}{mol}$
Injection Number	$\underline{In} := 30$	
Peak Area Sum	$\Sigma pa := 4260$ [pA]	
Avogadro's Number	$A_a := 6.022 \cdot 10^{23}$ $\left(\frac{atoms}{mol}\right)$	
Stoichiometric ratio	$X_m := 1$ [mol H2 per mol of Pd]	
Atoms of Pd per Area	$\underline{ns} := 1.27E+19$ $\left(\frac{atoms}{m^2}\right)$	
	or	
	$nsn := \frac{ns}{A_a}$ $\left(\frac{mols}{m^2}\right)$	
	$nsn = 2.109 \times 10^{-5}$ $\left(\frac{m^2}{m^2}\right)$	
Theoretical amount of Pd moles	$N_{pd} := N_s \cdot 30$ [mol]	
Moles of H2 adsorbed per gram of sample	$N_m := N_{pd} - \left[\frac{(\Sigma pa \cdot N_s)}{A_b}\right]$	
Atheory := $\left[\left(\frac{wt}{Pd_{mw}}\right) \cdot \left(\frac{A_a}{ns}\right)\right]$	Atheory = 44.557 $\left(\frac{m^2}{gram\_Catalyst}\right)$	

Calculations of the first 80 C run:

$R_x := \frac{N_s}{A_b} = 5.475 \times 10^{-10}$ $\left(\frac{mol}{pA}\right)$	
$N_{pd} = 2.628 \times 10^{-6}$	
$N_m = 2.956 \times 10^{-7}$	
$Ad_{sum} := N_m$ (mol)	
$At_{sum} := Ad_{sum} \cdot A_a = 1.78 \times 10^{17}$ (atoms)	$A = 23.365$ $\left(\frac{m^2}{gram\_Catalyst}\right)$
$\underline{Ai} := \frac{(At_{sum} \cdot X_m)}{ns} = 0.014$ $\left(m^2\right)$	Dispersion
convert to per gram of sample:	$D := \frac{A}{A_{theory}} = 0.524$ Percent := D-100 = 52.438 %
$\underline{A} := \left[\frac{1}{(0.0006)}\right] \cdot Ai$ $\left(m^2\right)$	

## 8.2 Titration Data Excerpt

**Table 6:** Average amount of Hydrogen injected for each single titration under various temperatures

	Averaged 40	Averaged 80	Averaged 120	Blank 80 C
1	81.29	98.32	73.38	-1.531635314
2	52.35	60.86	12.43	-1.265263955
3	30.38	36.88	0.14	-0.799114077
4	15.29	22.22	-3.82	-0.665928397
5	12.17	18.13	-4.07	-0.532742718
6	11.51	18.06	-4.63	0.199778519
7	10.06	16.76	-6.31	0.266371359
8	8.80	15.35	-3.94	0.799114077
9	9.88	16.66	-4.63	0.732521237
10	3.89	12.06	-6.56	0.665928397
11	59.71	48.03	32.73	2.463935071
12	7.21	12.49	1.76	1.798006673
13	7.07	7.59	0.45	1.664820994
14	5.22	5.72	0.25	1.664820994
15	3.09	7.08	-1.91	1.798006673
16	3.50	3.93	-1.88	1.864599513
17	1.94	6.18	-2.61	1.798006673
18	3.22	8.12	-1.95	1.931192353
19	2.76	5.77	-3.34	1.864599513
20	3.65	5.81	-1.60	1.864599513
21	24.17	36.98	43.15	0.133185679

22	4.69	5.63	5.03	-0.06659284
23	0.09	3.09	2.16	-0.133185679
24	-1.11	3.05	0.38	-0.266371359
25	0.98	4.01	0.26	-0.199778519
26	0.45	3.53	-0.43	-1.89268E-14
27	-1.01	2.47	-1.35	-0.199778519
28	0.69	-1.80	-0.26	-0.266371359
29	0.16	-0.45	0.74	0.133185679
30	-0.72	2.25	-0.31	0.133185679

**Table 7:** Valve Injection Time - Further Mass Limitation Testing

Titration	Peak area	Injection time (min)
1	35	4
2	40.1	10
3	67.8	10
4	50.1	10
5	50	15
6	49.6	15
7	49.5	20
8	50.9	20
9	59.6	25
10	49.6	25
11	42.7	30
12	47.3	32
13	47	4
14	49.8	10
15	48.7	10
16	49.5	10
17	51.8	15
18	62	15
19	51.2	20

20	50	20
21	50.8	25
22	58.4	25
23	51.8	30
24	54.6	4
25	53.2	10
26	55.3	10
27	50.7	10
28	53.2	15
29	54.3	15
30	51.6	20

### 8.3 SEM

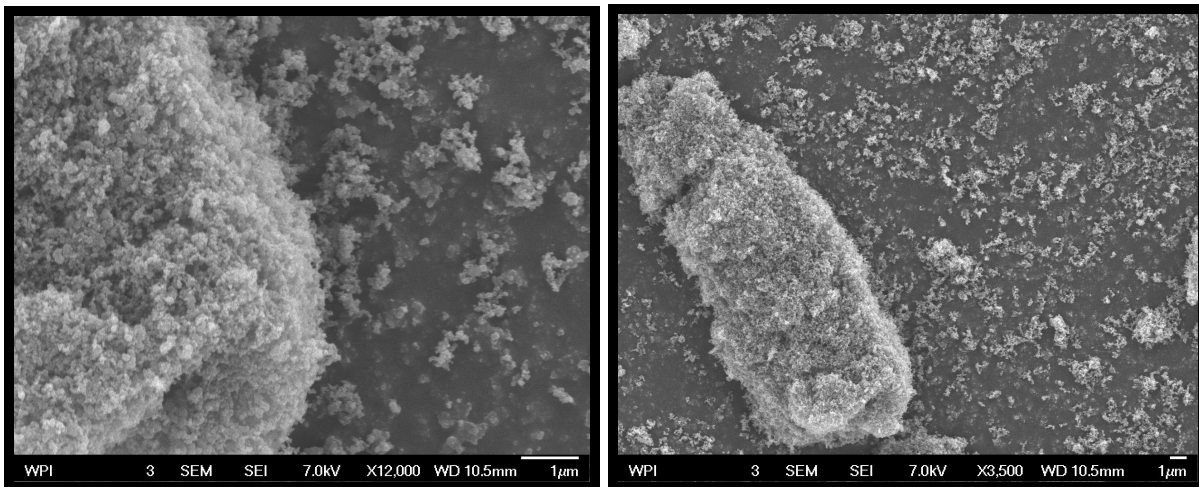


**Figure 32: Left.** Palladium on Vulcan Fresh x12,000. **Right.** Palladium on Vulcan Fresh x3500

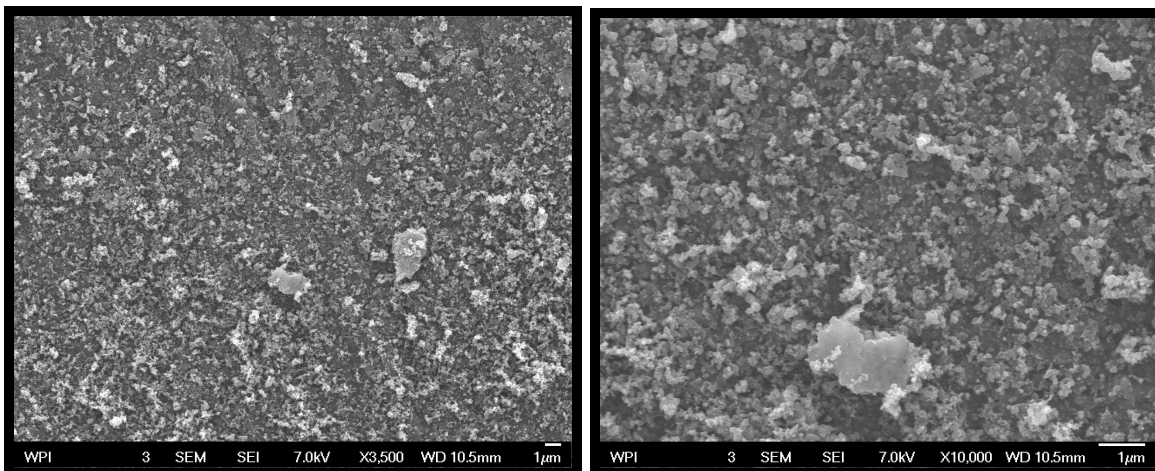


**Figure 33: Left.** Palladium on Vulcan BET x3500. **Right.** Palladium on Vulcan BET x10,000

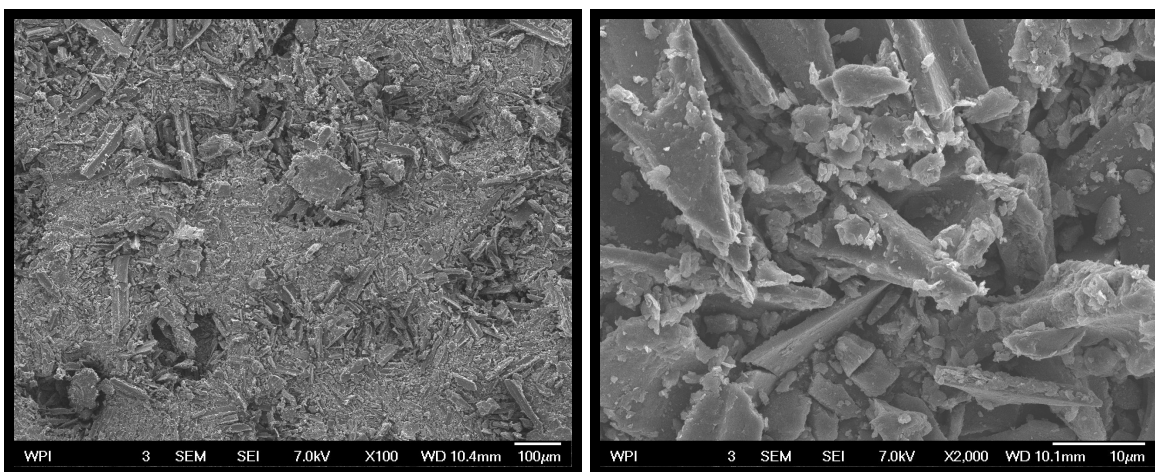


**Figure 34: Left.** Palladium on Carbon Fresh x100. **Right.** Palladium on Carbon Fresh x2000

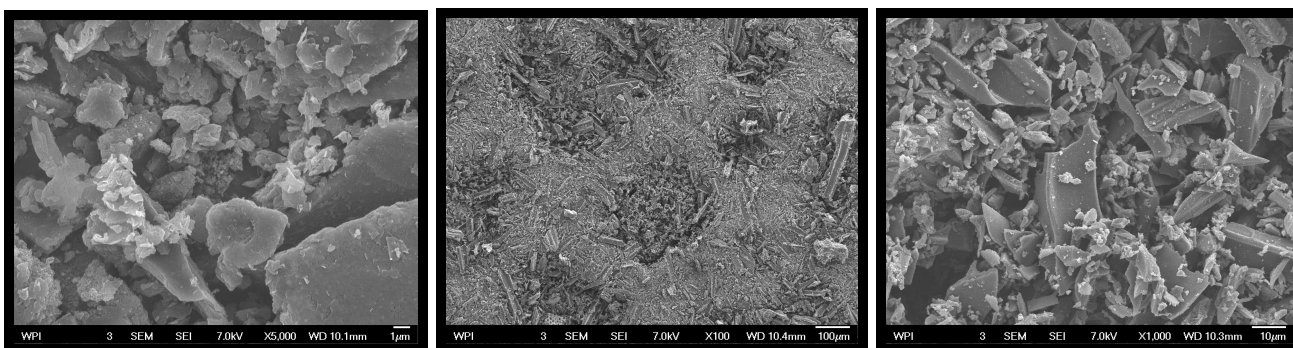


**Figure 35: Left.** Palladium on Carbon Fresh x5000. **Middle.** Palladium on Carbon Spent x100. **Right.** Palladium on Carbon Spent x1000

**Table 8:** SEM image Palladium on Carbon Spent scan 1000x zoom Percent Error.

Number	Length in micrometers
1	37.769
2	35.932
3	35.326
4	35.911
5	34.309
6	31.124
7	33.867
8	30.537
9	35.46
10	33.284
AVG	34.3519
MAX	37.769
MIN	30.537

## 8.4 Valve Configurations

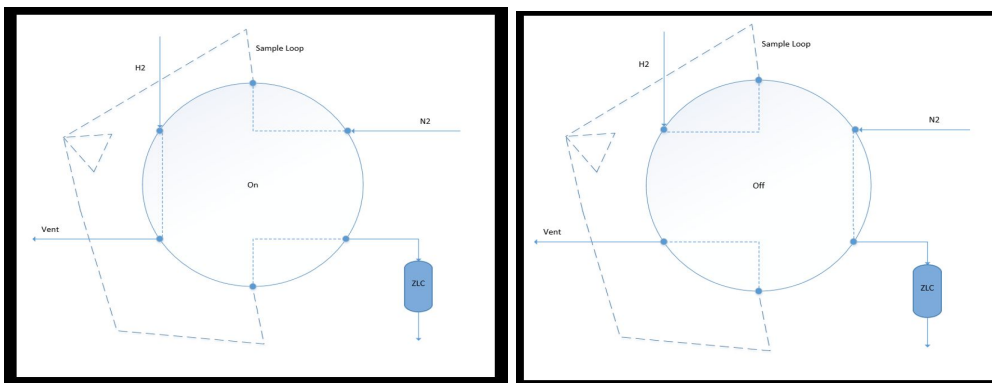


**Figure 36:** Left. Chemisorption valve configuration of Injection state. Right. Chemisorption valve configuration of Loading state

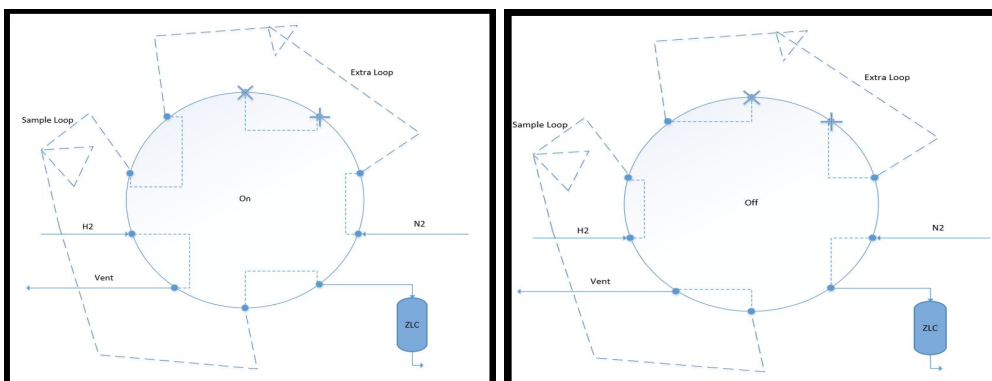


**Figure 37:** Left. 10 Port valve configuration of injection state. Right. 10 Port valve configuration of loading state

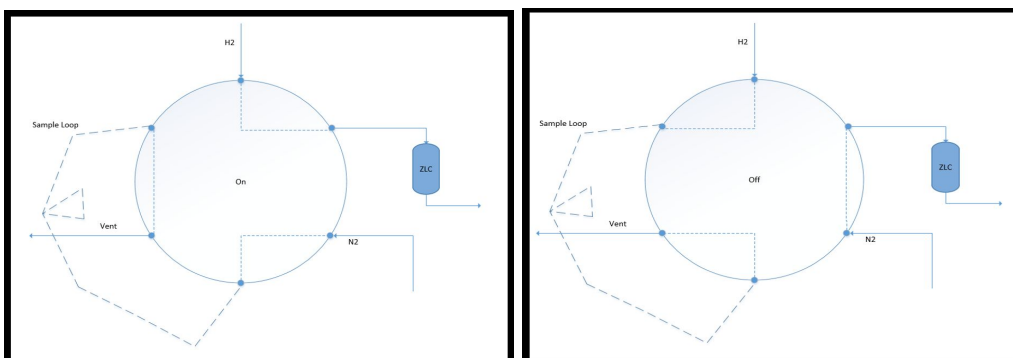


**Figure 38:** Left. ZLC experiment valve configuration of Nitrogen constant flow state. Right. ZLC experiment valve configuration of Hydrogen constant flow state.

## 8.5 MatLAB Script

```
Finding Beta%%.....
4
solving for diffusivity %%.....
5
clc
clear
close all

files = dir('3TPD45-4-9-.txt')
%2TPD15-4-9-.txt
%3TPD45-4-9-.txt
%1TPD60-4-9-.txt
vector= [1]
vectorsz= size(vector,1);

for i= 1:numel(files)
data= dlmread(files(i).name);

%pull column two
y= data(:,2);

%find end length of data sheet - since the y column is typically one or two
%rows shorter than the time column.
yl = size(y,1)

%pull column one
x= data(1:yl,1);

t= data(1:yl,1);
%normalize time

tnrm= x-45; % NEEDS TO BE ADJUSTED BASED ON EXPERIMENT TIME
%find row when t=0
t0= find(tnrm.^2 == min(tnrm.^2));

%normalize y column data
%adjust 1.1 below to reach the sensitivity at a certain run.
y(end);
if y(end) ~= 0
```

```

ye = 0.9.*y(end-1);
else
ye = 0.9.*y(end-1,1);
end
ye
yinf= vector(i)*ye;
y0= y(t0,end);
ynrm= ((y-yinf)/(y0-yinf));

```

```

figure(1)
hold on
plot(t,y)
xlabel('Time, [s]')
ylabel('RAW Signal Intensity')

```

```

figure(2)
hold on
semilogy(tnrm,ynrm)
legendInfo{i} = ['Run = ' num2str(i)];
set(gca,'yscale','log')
%Adjust Axis Below
axis([0.5 1.2 1e-8 1])
xlabel('Desorption Time, [s]')
ylabel('c/c-0, [ - ]')
% X Y Data for plotting

%clean up workspace
clear t t0 y y0 yinf
end

```

files =

struct with fields:

```

name: '3TPD45-4-9-.txt'
folder: 'C:\Users\Jonathan\Documents\Senior Year\MQP\2 TPR'
date: '12-Apr-2018 09:17:12'
bytes: 6396332
isdir: 0
datenum: 7.3716e+05

```

```
vector =
```

```
1
```

```
yl =
```

```
180002
```

```
ye =
```

```
-59.4026
```

```
Warning: Negative data ignored
```

## Finding Beta%%

```
%FIND LINEAR REGION ON THE GRAPH PLOTTED ABOVE
```

```
tti = find(tnrm == 0.7)
```

```
tff = find(tnrm == 1)
```

```
[~,tti] = min((tnrm-0.7).^2);
```

```
[~,tff] = min((tnrm-1).^2);
```

```
%extract row data
```

```
T = tnrm(tti:tff,1);
```

```
C = ynrm(tti:tff,1);
```

```
%find the slope and intercept
```

```
polyfit(T,log(C),1)
```

```
%find beta based on intercept
```

```
coeff = polyfit(T,log10(C),1);
```

```
plot ([0 T'],10.^polyval(coeff,[0 T']),'r:')
```

```
goal = coeff(1,2)
```

```
b = 2:0.001:3.14;
```

```
%Equation for the intercept
```

```
F = (log10((2.*((1-b)./tan(b)))/b.^2+((1-b)./tan(b).*((1-b)./tan(b)-1))));
```

```
%%%CAUTION ABOVE IS AN EQUATION BASED ON A SPHERICAL SHAPE%%%
```

```
%Function of F and goal ---- includes error
```

```
fun = (F+goal).^2;
```

```
%creat an index for less than the minimum value output for function
```

```
[~,index] = min(fun)
```

```
%Beta is equal to the beta value at the respevtive index in previous line
```

```
Beta = b(index)
```

```
clear goal
```

```
tft =
```

```
0×1 empty double column vector
```

```
tff =
```

```
0×1 empty double column vector
```

```
ans =
```

```
-11.0088    2.8628
```

```
goal =
```

```
1.2433
```

```
index =
```

```
26
```

```
Beta =
```

2.0250

## solving for diffusivity %%

```
%Length of Graphite Slab in cm
```

```
L = 0.000643;
```

```
%goal now set to equal the slope
```

```
goal = coeff(1,1)
```

```
%equation solved for diffusivity
```

```
D = -(goal.*L.^2)/Beta.^2
```

```
figure;
```

```
plot(F)
```

```
goal =
```

```
-4.7811
```

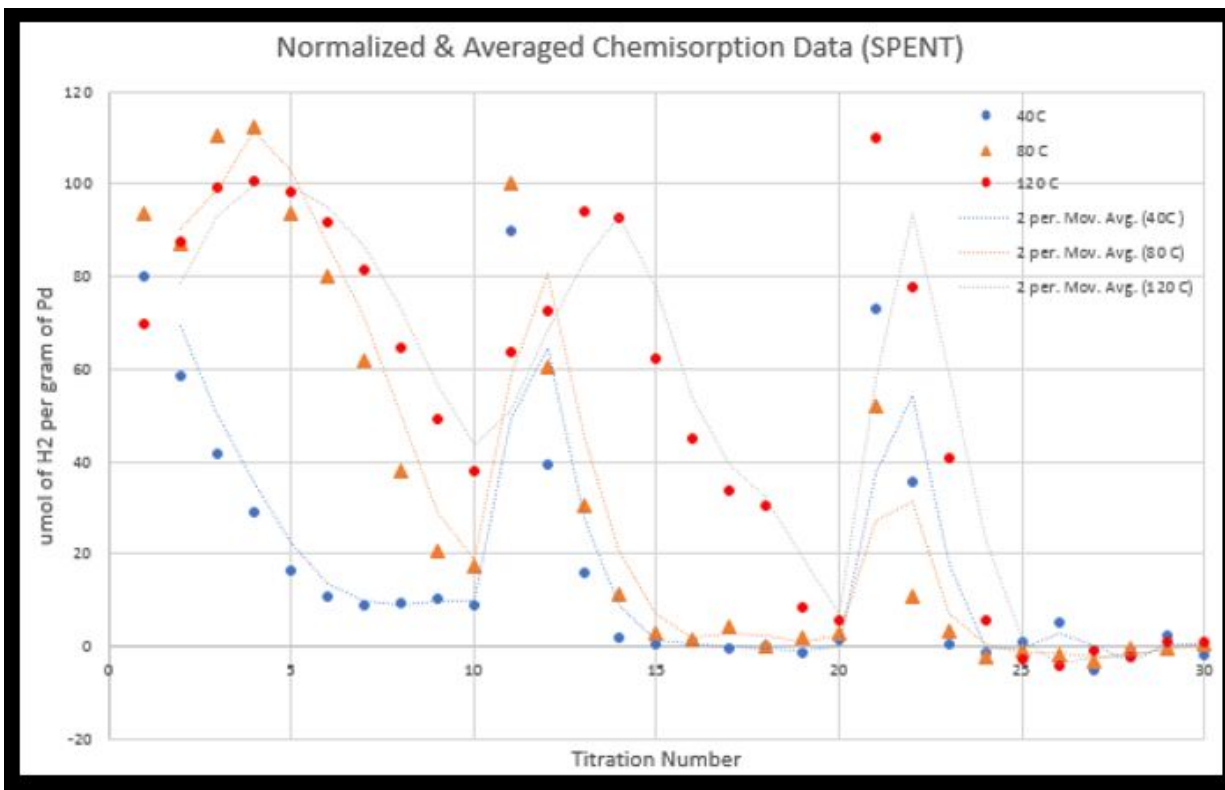
```
D =
```

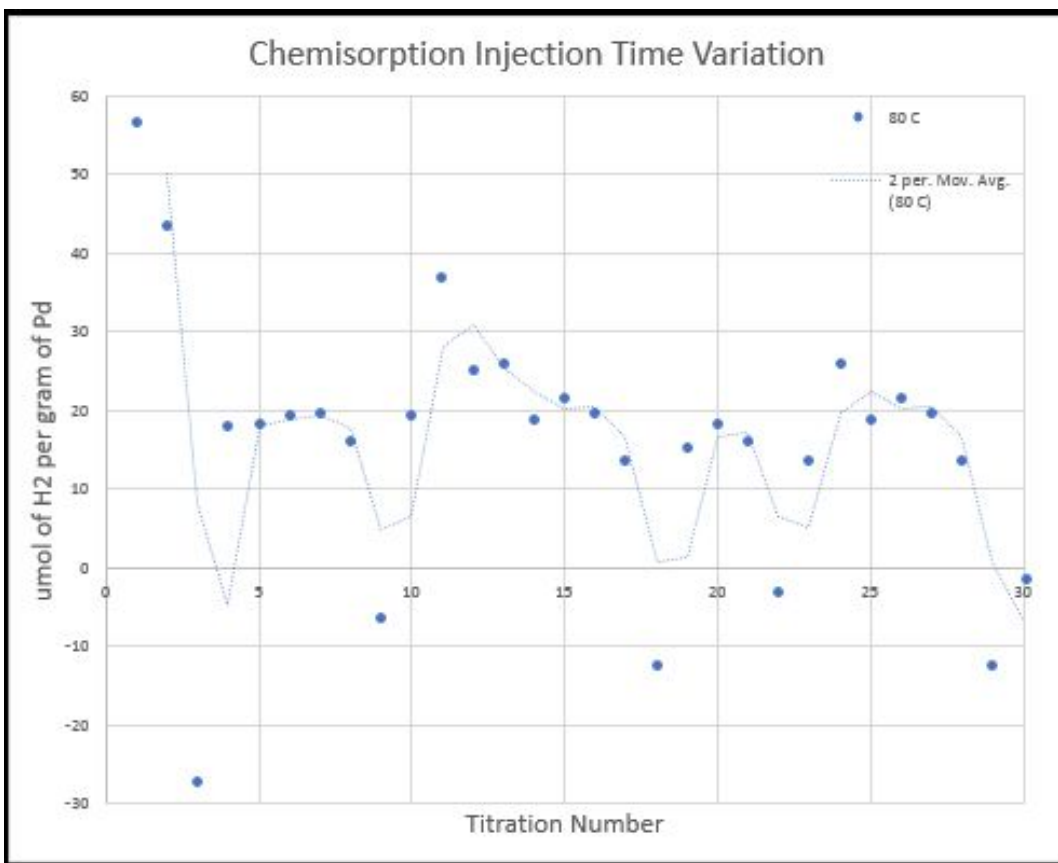
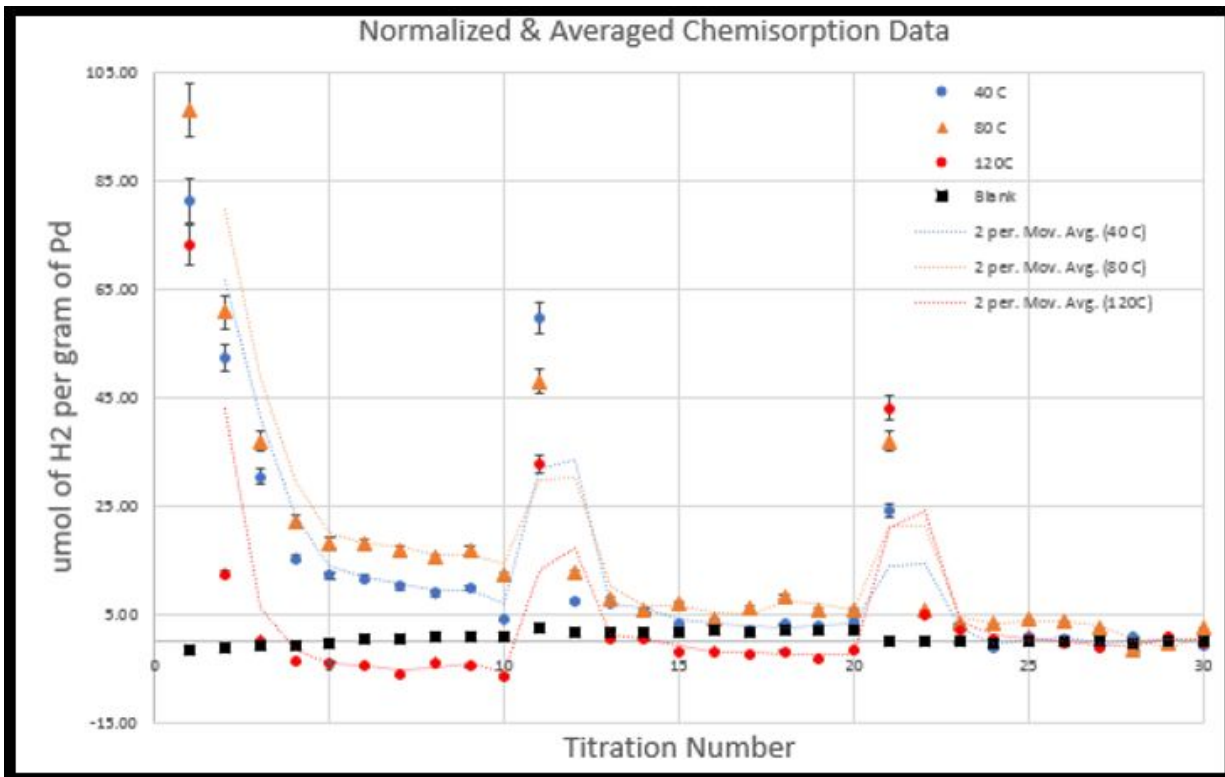
```
4.8205e-07
```

*Published with MATLAB® R2017a*

## 8.6 Chemisorption Graphs

Chemisorption Graphs in order: Spent Averaged, Fresh Averaged, and 80 C Fresh with variance in injection time.





## 9. References

1. J.A Mouljn, A.Evan Diepen, F Kapteijn. (2001) Catalyst deactivation: is it predictable?: What to do?. *Applied Catalysis A: General*. From: <https://www.sciencedirect.com/science/article/pii/S0926860X00008425>
2. G. Ertl, H. Knozinger and J. Weitkamp (Eds.), *Handbook of Heterogeneous Catalysis* (1997), VCH, Weinheim.
3. "Platinum" Support. Vol. A 1, 1985, pp. 225/7.
4. Satish M. Manocha. (2003). Porous Carbon. *Sadhana Academy Proceedings In Engineering Science*. From <https://link.springer.com/content/pdf/10.1007/BF02717142.pdf>
5. U.A.Paulus, T.J.Schmidt, H.A.Gasteiger, R.J.Behm (2001). Oxygen reduction on a high-surface area Pt/Vulcan carbon catalyst: a thin-film rotating ring-disk electrode study. *Journal of Electroanalytical Chemistry*. From <https://www.sciencedirect.com/science/article/pii/S0022072800004071>
6. Manish Chandra, Qiang Xu (2007). Room temperature hydrogen generation from aqueous ammonia-borane using noble metal nano-clusters as highly active catalyst. *Journal of Power Sources*. From <https://www.sciencedirect.com/science/article/pii/S0378775307005605>
7. Jennifer Lew. (2016) Catalytic Hydrogenation of Alkenes. *Chemistry LibreTexts*. From [https://chem.libretexts.org/Core/Organic\\_Chemistry/Alkenes/Reactivity\\_of\\_Alkenes/Catalytic\\_Hydrogenation](https://chem.libretexts.org/Core/Organic_Chemistry/Alkenes/Reactivity_of_Alkenes/Catalytic_Hydrogenation)
8. James. Reagent Friday: Palladium on Carbon (Pd/C). *Master Organic Chemistry*. From <https://www.masterorganicchemistry.com/2011/11/25/palladium-on-carbon-pdc/>
9. Boskovic, G., & Baerns, M. (2004). Catalyst Deactivation . *Basic Principles in Applied Catalysis*. Retrieved February 28, 2018, from [https://link.springer.com/content/pdf/10.1007%2F978-3-662-05981-4\\_14.pdf](https://link.springer.com/content/pdf/10.1007%2F978-3-662-05981-4_14.pdf).

10. Aigin Zhang, e. a. (2014). Homogeneous Pd nanoparticles produced in direct reactions: green synthesis, formation mechanism and catalysis properties. *Journal of Materials Chemistry A*, Electric.
11. Amorim, C., & Keane, M. (2008). Palladium supported on structured and nonstructured carbon: A consideration of Pd particle size and the nature of reactive hydrogen. *Journal of Colloid and Interface Science*, 197- 208.
12. BASF. (2017, February 27th). *Engelhard Industrial Bullion (EIB) Prices*. From BASF Catalysts: <https://apps.catalysts.basf.com/apps/eibprices/mp/>
13. *Catalysis in industry*. (2013, May 10). From The Essential Chemical Industry - online: <http://www.essentialchemicalindustry.org/processes/catalysis-in-industry.html>
14. Duncan, W., & Moller, K. (2000). A 'zero length' criterion for ZLC chromatography. *Chemical Engineering Science*, 5415-5420.
15. I. Chorkendorff, J. N. (2007). *Concepts of Modern Catalysis and Kinetics*. Federal Republic of Germany: Deutsche Nationalbibliothek.
16. Pearson. (2002). *Chemical Reactions*. From PrenHall: [http://wps.prenhall.com/wps/media/objects/376/385232/Media-Portfolio/chapter\\_07/07.html](http://wps.prenhall.com/wps/media/objects/376/385232/Media-Portfolio/chapter_07/07.html)
17. Quantachrome Instruments. (2009-2013). *Characterizing Porous Materials and Powders: Operation Manual - TPRWin ver. 3.5*. Quantachrome Instruments.
18. Sariođlan, S. (2013). Recovery of Palladium from Spent Activated Carbon-Supported Palladium Catalysts. *Platinum Metals Rev*.
19. STREM Chemicals. (n.d.). *High Performance Carbon Supported Palladium Catalysts for Hydrogenation*. From [https://www.strem.com/uploads/resources/documents/high\\_performance\\_carbon\\_supported\\_palladium\\_catalysts\\_for\\_hydrogenation.pdf](https://www.strem.com/uploads/resources/documents/high_performance_carbon_supported_palladium_catalysts_for_hydrogenation.pdf)
20. T. Armaroli, T. B. (2004). Diffuse Reflection Infrared Spectroscopy (DRIFTS): Application to the in situ Analysis of Catalysts. *Oil & Gas Science and Technology – Rev. IFP, Vol. 59 (2004)*, 215-237.

21. Thorsten Wagner, e. a. (2011). A High Temperature Capacitive Humidity Sensor Based on Mesoporous Silica. *Sensors*, Electronic.
22. Wagner, T. (2011). A High Temperature Capacitive Humidity Sensor Based on Mesoporous Silica. *Sensors*, [www.mdpi.com/journal/sensors](http://www.mdpi.com/journal/sensors).
23. Wolf, R. (2013, August 13). *What is ISP-MS*. From USGS: <https://crustal.usgs.gov/laboratories/icpms/intro.html>
24. Peter Munnik, Petra E. de Jongh, and Krijn P. de Jong. (2015). Recent Developments in the Synthesis of Supported Catalysts. *Chemical Review*. From <https://pubs.acs.org/doi/pdfplus/10.1021/cr500486u>
25. Busacca, C. A., Fandrick, D. R., Song, J. J., & Senanayake, C. H. (2011). The Growing Impact of Catalysis in the Pharmaceutical Industry. *Advanced Synthesis & Catalysis*, 353(11-12), 1825-1864. doi:10.1002/adsc.201100488
26. Thomas, J. M. (2012). ChemInform Abstract: The Societal Significance of Catalysis and the Growing Practical Importance of Single-site Heterogeneous Catalysts. *ChemInform*, 43(48). doi:10.1002/chin.201248250
27. Argyle, M., & Bartholomew, C. (2015, February 26). Heterogeneous Catalyst Deactivation and Regeneration: A Review. Retrieved from <http://www.mdpi.com/2073-4344/5/1/145/htm>
28. Forzatti, P. (1999). Catalyst deactivation. *Catalysis Today*, 52(2-3), 165-181. doi:10.1016/s0920-5861(99)00074-7
29. Munnik, P., Jongh, P. E., & Jong, K. P. (2015). ChemInform Abstract: Recent Developments in the Synthesis of Supported Catalysts. *ChemInform*, 46(38). doi:10.1002/chin.201538284
30. Hunt, I. R. (n.d.). Protecting Groups. Retrieved from <http://www.chem.ucalgary.ca/courses/350/Carey5th/Ch17/ch17-3-4-3.html>
31. Palladium (Pd) Catalysts. (n.d.). Retrieved from <https://www.sigmaaldrich.com/chemistry/chemistry-products.html?TablePage=1624796>

32. Catalyst Supports and Carriers Information. (n.d.). Retrieved from [https://www.globalspec.com/learnmore/materials\\_chemicals\\_adhesives/chemicals\\_raw\\_materials/catalyst\\_supports\\_carriers](https://www.globalspec.com/learnmore/materials_chemicals_adhesives/chemicals_raw_materials/catalyst_supports_carriers)
33. Lam, E., & J. L. (n.d.). Carbon Materials as Catalyst Supports and Catalysts in the Transformation of Biomass to Fuels and Chemicals. Retrieved from <https://pubs.acs.org/doi/abs/10.1021/cs5008393>
34. Zhang, A., Liu, M., Liu, M., Xiao, Y., Li, Z., Chen, J., . . . Li, F. (2013, December 10). Homogeneous Pd nanoparticles produced in direct reactions: Green synthesis, formation mechanism and catalysis properties. Retrieved from <http://pubs.rsc.org/en/content/articlelanding/2014/ta/c3ta14299j/unauth#!divAbstract>
35. Eic and Ruthven. (1987, June 8). *A New Experimental Technique for Measurement of Intracrystalline Diffusivity*. Department of Chemical Engineering, University of New Brunswick, Canada.
36. Lew, J. (2016, November 29). Catalytic Hydrogenation of Alkenes. Retrieved from [https://chem.libretexts.org/Core/Organic\\_Chemistry/Alkenes/Reactivity\\_of\\_Alkenes/Catalytic\\_Hydrogenation](https://chem.libretexts.org/Core/Organic_Chemistry/Alkenes/Reactivity_of_Alkenes/Catalytic_Hydrogenation)